

# Pairwise maximum-entropy models and their Glauber dynamics: bimodality, bistability, non-ergodicity problems, and their elimination via inhibition

Vahid Rostami <sup>1\*</sup>, PierGianLuca Porta Mana <sup>1</sup>, Moritz Helias <sup>1,2</sup>

16 May 2016

<sup>1</sup> Institute of Neuroscience and Medicine (INM-6) and Institute for Advanced Simulation (IAS-6) and JARA BRAIN Institute I, Jülich Research Centre, Germany

<sup>2</sup> Department of Physics, Faculty 1, RWTH Aachen University, Germany

\* v.rostami@fz-juelich.de

## Abstract

Pairwise maximum-entropy models have been used in recent neuroscientific literature to predict the activity of neuronal populations, given only the time-averaged correlations of the neuron activities. This paper provides evidence that the pairwise model, applied to experimental recordings, predicts a bimodal distribution for the population-averaged activity, and for some population sizes the second mode peaks at high activities, with 90% of the neuron population active within time-windows of few milliseconds. This bimodality has several undesirable consequences: 1. The presence of two modes is unrealistic in view of observed neuronal activity. 2. The prediction of a high-activity mode is unrealistic on neurobiological grounds. 3. Boltzmann learning becomes non-ergodic, hence the pairwise model found by this method is not the maximum entropy distribution; similarly, solving the inverse problem by common variants of mean-field approximations has the same problem. 4. The Glauber dynamics associated with the model is either unrealistically bistable, or does not reflect the distribution of the pairwise model. This bimodality is first demonstrated for an experimental dataset comprising 159 neuron activities recorded from the motor cortex of macaque monkey. Using a reduced maximum-entropy model, evidence is then provided that this bimodality affects typical neural recordings of population sizes of a couple of hundreds or more neurons. As a way to eliminate the bimodality and its ensuing problems, a modified pairwise model is presented, which – most important – has an associated pairwise Glauber dynamics. This model avoids bimodality thanks to a minimal asymmetric inhibition. It can be interpreted as a minimum-relative-entropy model with a particular prior, or as a maximum-entropy model with an additional constraint. The bimodality problem, the modified maximum-entropy model, and the question of the relevance of pairwise correlations are presented and discussed from the general perspective of predicting activity given stimuli, formalized in simple mathematical terms.

## Author summary

Networks of interacting units are ubiquitous in various fields of biology (gene regulatory networks, neuronal networks, social structure). If a limited set of observables is accessible, maximum entropy models provide an unbiased way to construct a statistical model. The pairwise model only uses the first two moments among those observables as constraints and therefore yields units that interact in a pairwise manner. Already at this level, a fundamental problem arises: if correlations are on average positive, we here show that the maximum entropy distribution tends to become bimodal. In the application to neuronal activity, the bimodality is an artefact of the statistical model. We here explain under which conditions bimodality arises and present a solution to the problem by introducing a path of collective negative feedback. This result may point to the existence of a homeostatic mechanism active in the system that is not part of our set of observable units.

## 1 Introduction

Understanding the relation between brain activity on one side, and what we could call the “state” of the brain – the complex combination of behaviour, stimuli, memory, and thought, which still partly escapes definition and measurement [1] – on the other side, is a major goal in the study of the brain [2, 3]. We would like to achieve this understanding at a probabilistic level at least. In very hand-waving terms, we could say it amounts to assigning probabilities of the form

$$P(\text{brain activity}|\text{state}). \quad (1)$$

Given the practically uncountable patterns of activity in the brain or even in just a small region of it, and the continuous spectrum and even vagueness of “states”, assigning such probabilities is practically impossible and will likely stay that way for the next few decades. In Bayesian theory we deal with a vague or too large set of probabilities by introducing one or more statistical models, which simplify the problem and give it well-defined contours. For example, we can introduce a set of models  $\{M\}$ , each of which includes some multi-dimensional parameter  $\alpha$ , in such a way that they informationally *screen off* every “brain activity” from every “state”,

making them conditionally independent [4–7]:

$$P(\text{activity} | \boldsymbol{\alpha}, M, \text{state}) = P(\text{activity} | \boldsymbol{\alpha}, M) \quad \text{for all activities and states.} \quad (2)$$

Then the inverse also holds:  $P(\text{state} | \boldsymbol{\alpha}, M, \text{activity}) = P(\text{state} | \boldsymbol{\alpha}, M)$ . By the rules of marginalization and total probability we can then rewrite the probability  $P(\text{activity} | \text{state})$  as

$$P(\text{activity} | \text{state}) = \sum_M \int P(\text{activity} | \boldsymbol{\alpha}, M) P(\boldsymbol{\alpha}, M | \text{state}) d\boldsymbol{\alpha}. \quad (3)$$

The advantage of this approach appears in the mutual information conditional on the model  $M$  and  $\boldsymbol{\alpha}$ :

$$I(\text{activity}, \text{stimuli} | \boldsymbol{\alpha}, M) = 0,$$

or, paraphrasing Caves [8]: “the mutual information between state and brain activity flows through the model  $M$  and parameters  $\boldsymbol{\alpha}$ ”. In this *divide et impera* approach we deal more easily with  $P(\text{activity} | \boldsymbol{\alpha}, M)$  and  $P(\boldsymbol{\alpha}, M | \text{stimuli})$  separately than with the full probability eq. (1), provided the parameter  $\boldsymbol{\alpha}$  has much fewer dimensions than the “activity” and “state” spaces. This parameter then constitutes a coarser but sufficient description of the activity, or of the state (stimuli, behaviour, memory, thought processes), or of both. An example of the first case could be the mean activities and pairwise correlations of a neuronal population; an example of the second could be the orientation of a light-intensity gradient on the retina, or ambient temperature. In the first case, if the model  $M$  can be interpreted and motivated neurobiologically, then it is a “neural code” [9–14].

The abstract viewpoint just outlined [see 6, 7, 15–20] is useful for understanding recent applications of the maximum-entropy method in neuroscience: the main topic of this paper is in fact a concrete example of this viewpoint where the model  $M$  is a maximum-entropy model [21–40, and references therein], and the parameter  $\boldsymbol{\alpha}$  is the empirical means and the pairwise empirical correlations of the activity of a neuronal population. Does such a choice of model and parameters give reasonable predictions  $P(\text{activity} | \boldsymbol{\alpha}, M)$ ? This question has been asked repeatedly in the neuroscientific literature of the

past few years. Some studies [e.g., 41–45] have tested the suitability of the maximum-entropy distribution – eq. (2) from our perspective – for various experimental and simulated “activities” and “states”. Some studies [e.g., 46–51] have tested the suitability of pairwise correlations or of higher-order moments – our parameter  $\alpha$ . Some studies have done both at the same time [52–55].

Computing the maximum-entropy distribution from moment constraints – this is usually called the *inverse problem* – is very simple in principle: it amounts to finding the maximum of a convex function [56–58]. The maximum can be searched for with a variety of methods (downhill simplex, direction set, conjugate gradient, etc. [59, ch. 10]). The convex function, however, involves a sum over  $\exp(\text{number of neurons})$  terms. For 60 neurons, that is roughly twice the universe’s age in seconds, but modern technologies enable us to record from *hundreds* of neurons simultaneously [60–62]. The convex function must therefore be “sampled” rather than calculated, usually via Markov chain Monte Carlo techniques [59, 63–68]. In neuroscience the Glauber dynamics (also known as Gibbs sampling) [65, 69, chap. 29] is usually chosen as the Markov chain whose stationary probability distribution is the maximum-entropy one.

*Boltzmann learning* [70–72] is such an iterative combination of sampling and maximum search, and is still considered the most precise method of computing a maximum-entropy distribution – at least in the neurosciences, to which our knowledge on such methods is confined.

A different approach is to approximate the convex function with an analytic expression, and to find the maximum directly via the study of the derivatives of this approximation. The mean-field [73–75], Thouless-Anderson-Palmer [75, 76], and Sessak-Monasson [77, 78] approximations are examples of this approach, widely used in neuroscience. These approximations are valid only in limited regions of the domain of the original convex function, and their goodness is usually checked against a Boltzmann-learning calculation (as e.g. in Roudi et al. [52]).

Outside of Bayesian theory, moment-constrained maximum-entropy models have also been used in frequentist methods [79, 80] as generators of surrogate activity data, again via a Glauber dynamics. Such surrogates are

used as “null hypotheses” of independence or pairwise dependence between spike trains [81–85].

The pairwise maximum-entropy model has been used for *experimentally* recorded activities of populations of a couple hundreds neurons at most, so far; but its success (or lack thereof) cannot be automatically extrapolated to larger population sizes. Roudi et al. [86] gave evidence that the maximized Shannon entropy and other comparative entropies of such model may present qualitatively different features above a particular population size. This is possibly also the message of Tkačik, Mora, et al. [43, 87–89] in terms of “criticality”. (Note that any “criticality” in such models is not a physical property of the population activity, but of our uncertainty about it. Some choices of models or constraints may lead to a “critical” distribution, other choices may not.)

In the present paper we discuss a feature of the pairwise maximum-entropy model that may be problematic or undesirable: the marginal distribution for the population-averaged activity becomes *bimodal*, and one of the modes may peak at high activities. In other words, maximum-entropy predicts that the population should fluctuate between a regime with a small fraction of simultaneously active neurons, and another regime with a higher fraction of simultaneously active neurons; the fraction of the second regime be as high as 90%. This feature of the maximum-entropy model seems to have been observed before [41, 48, 90], but never remarked upon.

We also provide evidence that this bimodality is not just a mathematical quirk: it is bound to appear in applications to populations of more than a hundred neurons.

The bimodality makes the pairwise maximum-entropy model problematic, for several reasons.

First, from data reported in the neuroscientific literature [e.g., 44] the coexistence of two regimes appears neurobiologically unrealistic – the more so if the second regime corresponds to 90% of all units being active.

Second, two complementary problems appear with the Glauber dynamics and the Boltzmann-learning used to find the model’s parameters. If the minimum between the two probability maxima is shallow, the activity alternately hovers about either regime for *sustained* periods, which is again unrealistic,

and hence rules out this method to generate meaningful surrogate data. If the minimum between the two maxima is deep, the Glauber dynamics becomes practically *non-ergodic*, and the pairwise model *cannot be calculated at all* via Boltzmann learning or via the approximations previously mentioned [cf. 66, § 2.1.3][65, chap. 29]. This case is particularly subtle because it can go undetected: the non-ergodic Boltzmann learning still yields a reasonable-looking distribution, and this distribution gives back the moments used as constraints when re-checked with Monte Carlo sampling. However, *this distribution is not the sought pairwise maximum-entropy distribution*: the two differ quantitatively also for low activities. This subtle, misleading self-consistency makes us wonder whether some papers that apply the model to large populations are affected by the non-ergodicity, so that what they find and use is actually not a pairwise maximum-entropy distribution.

The plan of this paper is the following: after some mathematical and methodological preliminaries we show the appearance of the bimodality problem with an experimental dataset: the activity of 159 neurons recorded from macaque motor cortex. Then we use an analytically tractable homogeneous pairwise maximum-entropy model (called “reduced” model for reasons explained later) to give evidence that the bimodality affects larger and larger ranges of datasets as the population size increases. For example, if the observed Pearson correlations have a population-average larger than 0.05, the bimodality is bound to appear for population sizes of 500 neurons and above. We show that experimental datasets of neural-activity are likely to fall within the bimodality ranges. We also show that the bistability does not disappear in the inhomogeneous case – it may become worse.

After analysing the appearance of bimodality and the conditions for it, we also propose a way to eliminate it: using a slightly modified pairwise maximum-entropy distribution, which does not suffer from the bimodality problem. This modified distribution can be interpreted as arising from the principle of *minimum relative entropy* (also called minimum discrimination information) [e.g., 24, 26, 28, 34, 91–103] with respect to a neurobiologically motivated reference prior, or as a maximum-entropy distribution with an additional constraint. The most important property of this modified distribution is its stationarity under a modified Glauber dynamics that includes a minimal

*asymmetric inhibition*. In our eyes this gives a neurobiological justification for using the modified distribution and its Glauber dynamics. We also show that the modified maximum-entropy distribution is the actual one obtained via Boltzmann learning or other approximations in the non-ergodic case – and thus could be the distribution actually computed in papers that used such techniques.

We finally bring to a close with a summary about bimodality and its consequences, a justification of the modified maximum-entropy model and its reference prior, and on how these models and pairwise correlations fit within the modelling viewpoint outlined at the beginning of this section.

Some remarks and extensive references about maximum-entropy methodology are presented at relevant points in the paper.

Our terminology and mathematical notation conform as much as possible to ISO (and ANSI, NIST, DIN, JCGM) standards [104–111], in the hope of promoting and facilitating interdisciplinary communication.

## 2 Results

### 2.1 Preliminaries: maximum-entropy models and Glauber dynamics

Our study uses three main mathematical objects: the pairwise maximum-entropy distribution, a “reduced” pairwise maximum-entropy distribution, and the Glauber dynamics associated with them. We review them here and give some additional remarks and references that we have not seen elsewhere in the neuroscientific literature. Towards the end of the paper we will introduce an additional maximum-entropy distribution.

#### 2.1.1 Pairwise maximum-entropy model

First let us make mathematically clear what we mean by “activity”: a set of sequences of spikes of  $N$  neurons during a finite time interval  $[0, T]$ . These spike sequences are discretized: we divide the time interval into  $n$  bins of identical length  $\Delta$  equal to  $T/n$ , indexed by  $t$  in  $\{1, \dots, n\}$ . For each neuron  $i$ , the existence of one or more spikes in bin  $t$  is represented by  $s_i(t) = 1$ ,

and lack of spikes by  $s_i(t) = 0$ . With this binary representation, the activity of our population at time bin  $t$  is described by a vector:  $\mathbf{s}(t) := (s_i(t))$ . We will switch freely between vector and component notation for this and other quantities.

*Time* averages are denoted by a circumflex:  $\widehat{\cdot}$ , and *population* averages by an overbar:  $\bar{\cdot}$ . The activity summed over the population at time  $t$ , or *population-summed activity*, is denoted by  $S(t)$ , and the *population-averaged activity* by  $\bar{s}(t)$ :

$$S(t) := \sum_{i=1}^N s_i(t) \in \{0, 1, \dots, N\},$$

$$\bar{s}(t) := \frac{1}{N} \sum_{i=1}^N s_i(t) \equiv \frac{1}{N} S(t) \in \{0, 1/N, \dots, 1\}.$$

The time-averaged activity of neuron  $i$  is denoted by  $m_i$ :

$$m_i := \widehat{s_i(t)} := \frac{1}{T} \sum_{t=1}^n s_i(t), \quad (4)$$

and the time average of the product of the activities of the neuron pair  $ij$ , called *coupled activity*, is denoted by  $g_{ij}$ :

$$g_{ij} := \widehat{s_i(t) s_j(t)} := \frac{1}{T} \sum_{t=1}^n s_i(t) s_j(t). \quad (5)$$

These time averages are used as constraints for the maximum-entropy model, as presently explained.

The *pairwise* maximum-entropy statistical model [41, 46, 112, 113] assigns a time-independent probability distribution for the population activity  $\mathbf{s}(t)$  of the form (time is therefore omitted in the notation):

$$P_p(\mathbf{s} | \boldsymbol{\mu}, \boldsymbol{\Lambda}) = \frac{1}{Z_p(\boldsymbol{\mu}, \boldsymbol{\Lambda})} \exp\left(\sum_i \mu_i s_i + \sum_{i < j} \Lambda_{ij} s_i s_j\right),$$

$$Z_p(\boldsymbol{\mu}, \boldsymbol{\Lambda}) := \sum_{\mathbf{s}} \exp\left(\sum_i \mu_i s_i + \sum_{i < j} \Lambda_{ij} s_i s_j\right); \quad (6)$$

the Lagrange multipliers  $\boldsymbol{\mu}(\mathbf{m}, \mathbf{g})$  and  $\boldsymbol{\Lambda}(\mathbf{m}, \mathbf{g})$  are determined by enforcing the equality of the time averages eq. (4) and eq. (5) with the single- and

coupled-activity expectations, with their usual definitions

$$E_p(s_i) := \sum_{\mathbf{s}} s_i P_p(\mathbf{s}), \quad E_p(s_i s_j) := \sum_{\mathbf{s}} s_i s_j P_p(\mathbf{s}) \quad (7)$$

(or in matrix form  $E_p(\mathbf{s}) := \sum_{\mathbf{s}} \mathbf{s} P_p(\mathbf{s})$  and  $E_p(\mathbf{s} \mathbf{s}^\top) := \sum_{\mathbf{s}} \mathbf{s} \mathbf{s}^\top P_p(\mathbf{s})$ ):

$$E_p(s_i) = m_i \quad \text{and} \quad E_p(s_i s_j) = g_{ij}. \quad (8)$$

Noting that  $E_p(s_i) = P_p(s_i = 1)$ , and  $E_p(s_i s_j) = P_p(s_i = 1, s_j = 1)$ , we see that the constraints above are equivalent to fully fixing the single-neuron marginal probabilities of  $P_p$  and partly fixing its two-neurons marginal probabilities.

If we introduce the covariances  $\mathbf{c}$  and Pearson correlation coefficients  $\boldsymbol{\rho}$ ,

$$\begin{aligned} c_{ij} &:= E(s_i s_j) - E(s_i)E(s_j), \\ \rho_{ij} &:= \frac{c_{ij}}{\sqrt{[E_p(s_i^2) - E_p(s_i)^2][E_p(s_j^2) - E_p(s_j)^2]}}, \end{aligned} \quad (9)$$

the constraints above are jointly equivalent to

$$E_p(s_i) = m_i \quad \text{and} \quad c_{ij} = g_{ij} - m_i m_j \quad (10)$$

or

$$E_p(s_i) = m_i \quad \text{and} \quad \rho_{ij} = \frac{g_{ij} - m_i m_j}{\sqrt{(m_i - m_i^2)(m_j - m_j^2)}} \quad (11)$$

Note that the covariance constraints  $c_{ij} = g_{ij} - m_i m_j$  by themselves are not convex, i.e., they do not define a convex subset in the probability simplex on which the entropy is maximized. The Lagrange-multiplier method does not guarantee the uniqueness of the solution if *only* the covariances are constrained. Uniqueness has to be checked separately [31, 32, 40, 57, 114]. On the other hand, the constraints  $E_p(s_i) = m_i$  and  $E_p(s_i s_j) = g_{ij}$  are separately convex, thus their conjunction  $E_p(s_i) = m_i \wedge E_p(s_i s_j) = g_{ij}$  is convex too, and the bijective correspondence of the latter with  $E_p(s_i) = m_i \wedge c_{ij} = g_{ij} - m_i m_j$  guarantees that the latter set of constraints is convex as well. What we have said about the covariances  $\mathbf{c}$  also holds for the correlations  $\boldsymbol{\rho}$ .

It is important to remember that  $(\mathbf{m}, \mathbf{g})$  are physically measurable quantities, independent of the observer, whereas  $(E_p(s_i), E_p(s_i s_j))$  depend on

the observer’s uncertainty, quantified by her probability assignment, and are not physically measurable. Therefore the constraints eq. (8) are not trivial definitions (“:=”) or equivalences (“ $\equiv$ ”). In fact, in particular situations it does not make sense to enforce some of the constraints [115]; this also depends on *what is our uncertainty about*. Let us explain this point.

The maximum-entropy distribution represents our uncertainty about the population activity for each of the *given* time bins,  $t \in \{1, \dots, n\}$ ; this can be shown by symmetry and combinatorial arguments within the probability calculus [29–31, 33–35, 37, 40, 115–117]. Sometimes the maximum-entropy distribution is also used to represent someone’s uncertainty about a *new* observation about a new time bin, e.g.  $t$  equal to  $n + 1$ . But such use implies additional assumptions and a particular prior that are not always justified [115]. Here is an example: suppose the time average of the coupled activity of neurons 1 and 2 vanishes:  $g_{12} := \frac{1}{T} \sum_{t=1}^n s_1(t) s_2(t) = 0$  (this happens for a couple of pairs in our data). If we enforce the constraint  $E_p(s_1 s_2) = g_{12} = 0$ , then maximum-entropy says that it is *impossible* that neurons 1 and 2 spike together:  $P_p(s_1 = 1, s_2 = 1) = 0$  (the corresponding Lagrange multiplier  $A_{12} = -\infty$ ). This prediction makes sense if we are speaking about any of our  $n$  time bins – in fact,  $g_{12} = 0$  means that neurons 1 and 2 have never spiked together in our data, so the prediction is right. But it is an unreasonable prediction about a future or past time bin that is not part of our data: just because neurons 1 and 2 have not spiked simultaneously in our  $n$  data bins, we cannot conclude that it is *impossible* for them to spike or have spiked simultaneously in the future ( $t > n$ ) or in the past ( $t < 0$ ). Therefore, when some constraints assume extreme values, as  $g_{12} = 0$  in our example, it is not meaningful to use the maximum-entropy model for *new* predictions outside the given dataset. In this case it is more appropriate to use the full (Bayesian) probability calculus [65, 115, 118–122], possibly with maximum-entropy ideas on a more abstract level (space of prior distributions) [123–128].

Contrary to what is sometimes stated in the literature, it is not true that the maximum-entropy model can only be used if the time sequence of activities is “stationary”. This model represents a guess about the activities in the sequence, given *time-average* information. This guess, therefore, has to be time-invariant by symmetry: any time-dependent information has been erased

by the time averaging. In other words, it is our guess which is “stationary”, not the physical data; but it is still a good guess, given the time-independent information provided. With time-dependent constraints we would obtain a time-dependent maximum-entropy distribution [cf. 129]: this application of the maximum-entropy principle is called “maximum-calibre” [130–135].

### 2.1.2 Reduced maximum-entropy model

If the time-averaged activities  $\mathbf{m}$  are homogeneous, i.e. equal to one another and to their population average  $\bar{m}$ , and the  $N(N-1)/2$  time-averaged coupled activities  $\mathbf{g}$  are also homogeneous with population average  $\bar{g}$ ,  $\bar{g} := \frac{2}{N(N-1)} \sum_{i<j} g_{ij}$ , then the pairwise maximum-entropy distribution has homogeneous Lagrange multipliers by symmetry:  $\mu_i = \mu_r$  and  $\Lambda_{ij} = \Lambda_r$ . It reduces to the simpler and analytically tractable form

$$\begin{aligned} P_r(\mathbf{s} | \mu_r, \Lambda_r) &= \frac{1}{Z_r(\mu_r, \Lambda_r)} \exp[\mu_r N \bar{s} + \frac{1}{2} \Lambda_r N \bar{s} (N \bar{s} - 1)], \\ Z_r(\mu_r, \Lambda_r) &:= \sum_{\mathbf{s}} \exp[\mu_r N \bar{s} + \frac{1}{2} \Lambda_r N \bar{s} (N \bar{s} - 1)], \end{aligned} \quad (12)$$

which assigns equal probabilities to all those activities  $\mathbf{s}$  that have the same population average  $\bar{s}$ . In this homogeneous case, the values of the multipliers are equal to their averages:  $\mu_i = \mu_r = \bar{\mu} := \frac{1}{N} \sum_i \mu_i$  and  $\Lambda_{ij} = \Lambda_r = \bar{\Lambda} := \frac{2}{N(N-1)} \sum_{i<j} \Lambda_{ij}$ .

This simpler distribution could be interpreted as an approximation of the pairwise maximum-entropy one, achieved by disregarding the inhomogeneities. But it is also an exact maximum-entropy distribution in its own right, obtained by only constraining the expectations for the *population sums* of the single and coupled activities,

$$\sum_i s_i = S = N \bar{s}, \quad \sum_{i<j} s_i s_j = S(S-1)/2 = N \bar{s} (N \bar{s} - 1)/2,$$

to be equal to their measured time averages:

$$E_r(N \bar{s}) = N \bar{m} \quad \text{and} \quad E_r(N \bar{s} (N \bar{s} - 1)) = \frac{N(N-1)}{2} \bar{g} := \sum_{i<j} g_{ij} \quad (13)$$

(or equivalently constraining the population averages.)

For this reason we call the model eq. (12) a *reduced* (pairwise) maximum-entropy model. If the time-averages are homogeneous, then  $\mu_r = \bar{\mu} = \mu_i$ ,  $\Lambda_r = \bar{\Lambda} = \Lambda_{ij}$  and the reduced and full pairwise model coincide. But in the inhomogeneous case the multipliers of the reduced model are *not* equal to the averages of the pairwise one:  $\mu_r \neq \bar{\mu}$ ,  $\Lambda_r \neq \bar{\Lambda}$ .

It is straightforward to derive the probability distribution for the population average  $\bar{s}$  in this model, owing to its symmetry: if the average is  $\bar{s}$ , there must be  $N\bar{s}$  active neurons in the population, and there are  $\binom{N}{N\bar{s}}$  ways in which this is possible, all having equal probability given by eq. (12). Therefore,

$$P_r(\bar{s} | \mu_r, \Lambda_r) = \frac{1}{Z_r(\mu_r, \Lambda_r)} \binom{N}{N\bar{s}} \exp[\mu_r N\bar{s} + \frac{1}{2} \Lambda_r N\bar{s} (N\bar{s} - 1)],$$

$$Z_r(\mu_r, \Lambda_r) := \sum_{\bar{s}} \binom{N}{N\bar{s}} \exp[\mu_r N\bar{s} + \frac{1}{2} \Lambda_r N\bar{s} (N\bar{s} - 1)]. \quad (14)$$

This probability distribution  $P_r(\bar{s})$  can, in turn, also be obtained applying a minimum-relative-entropy principle [24, 34, 91–102], i.e. minimizing the relative entropy (or discrimination information)

$$H(P, P_0) := \sum_{\bar{s}} P(\bar{s}) \ln \frac{P(\bar{s})}{P_0(\bar{s})} \quad (15)$$

of  $P(\bar{s})$  with respect to the reference distribution  $P_0(\bar{s}) = 2^{-N} \binom{N}{N\bar{s}}$  while constraining the first two moments of  $P_r(S)$ , or equivalently its first two factorial moments [136],  $(E(S), E(S(S-1)/2))$ .

It is easy to see that in this model, by symmetry, we also have

$$E_r(s_i) = E_r(\bar{s}), \quad E_r(s_i s_j) = E_r\left(\frac{N\bar{s}(N\bar{s}-1)}{N(N-1)}\right), \quad (16)$$

$$c_{ij} = \bar{c} = E_r\left(\frac{N\bar{s}(N\bar{s}-1)}{N(N-1)}\right) - E_r(\bar{s})^2, \quad \rho_{ij} = \bar{\rho} = \frac{\bar{c}}{E_r(\bar{s}) - E_r(\bar{s})^2}, \quad (17)$$

and  $(E_r(\bar{s}), E_r(\frac{N\bar{s}(N\bar{s}-1)}{N(N-1)}))$ ,  $(E_r(\bar{s}), \bar{c})$ ,  $(E_r(\bar{s}), \bar{\rho})$  are equivalent sets of constraints (but  $\bar{c}$  and  $\bar{\rho}$  by themselves are not convex).

The reduced maximum-entropy model is mathematically very convenient, because the Lagrange multipliers  $\mu_r, \Lambda_r$  can be easily found numerically (with standard convex-optimization methods like downhill simplex, direction set,

conjugate gradient, etc. [59, ch. 10]) with high precision even for large (e.g., thousands) population sizes  $N$ .

Summarizing: the reduced maximum-entropy model can be seen as: 1. the form taken by the pairwise maximum-entropy model in the case of homogeneous single and couple activities; 2. an approximation to the pairwise maximum-entropy model in the case of inhomogeneous single and couple activities; 3. a maximum-entropy model in its own right, that uses less information than the full pairwise model.

### 2.1.3 Glauber dynamics

The maximum-entropy distributions above do not make any prediction about the dynamical or kinematical properties of the population activity, like first-passage times. They are, however, identical in form to the stationary distribution of an asynchronous Glauber dynamics [69] with symmetric “couplings”  $\mathbf{A}$ , sometimes interpreted as symmetric synaptic couplings, and “biases”  $\boldsymbol{\mu}$ , sometimes interpreted as either a threshold or external input controlling the base activity of individual neurons. In the reduced maximum-entropy model these parameters are homogeneous:  $A_{ij} = A_r$ ,  $\mu_i = \mu_r$ . The full and reduced maximum-entropy distributions give some information about this particular dynamics, like the appearance of metastable or most probable population-average states.

If we assume that our uncertainty about the *evolution* of the population activity can be modelled by the Glauber dynamics of a binary network, we can choose the  $\boldsymbol{\mu}, \mathbf{A}$  parameters determined by the constraints eq. (8) and thus generate surrogate data that – if the dynamics is ergodic – will have infinite-time-average activities as our initial experimentally observed data.

The formulae of the pairwise maximum-entropy model are similar or even identical to the formulae of the Lenz-Ising or Sherrington-Kirkpatrick spin model [137–143]. This similarity is useful: it allows us to borrow some mathematical techniques, approximations, and intuitive pictures developed for one model, and to apply them to the other. Yet we purposely emphasize the probability-calculus viewpoint and avoid any “explanation” via statistical-mechanical analogies and their related concepts and jargon. On the whole, such analogies are conceptually limitative and pedagogically detri-

mental because they put the logical cart before the logical horse: the logical route is not *statistical mechanics*  $\rightarrow$  *maximum-entropy*, but *probability calculus* + *physics*  $\rightarrow$  *maximum-entropy*  $\rightarrow$  *statistical mechanics* [144, chaps I–IV][25, 130, 132, 133, 145–153] [see also 154–157]. There are in fact important differences between the two models and their quantities. In no particular order:

First: in the case of the Lenz-Ising model, the microscopic state is unknown: we try to guess it from macroscopic properties; this is a problem of inference *within* a model (the energy-constrained maximum-entropy model itself is not brought into question). The opposite holds for the pairwise maximum-entropy model: the “microscopic state” (activity) is known, and we try to find the “macroscopic properties” that lead to a good guess about it; this is a problem of inference *of* a model [cf. 158].

Second: the Lenz-Ising model has one macroscopic quantity as constraint: the total energy, which has one associated Lagrange multiplier: the statistical temperature. The pairwise maximum-entropy model has  $N + (N^2 - N)/2$  constraints, with as many associated Lagrange multipliers. The difference of constraints between the two models implies essential differences between their entropies; negligence of such differences leads to variants of the Gibbs paradox [159–163].

Third: The couplings and external fields that appear in the energy of the Lenz-Ising model are measurable physical quantities. The mathematically similar Lagrange multipliers of the pairwise maximum-entropy model are statistical parameters and cannot be measured – they encode our ignorance. In particular, the expression “ $\sum_i \mu_i s_i + \sum_{i < j} A_{ij} s_i s_j$ ” – what Gibbs [144] calls *index of probability* – is *not* an energy. The following exercise shows why: Assume  $\mu_i = -3$ ,  $A_{ij} = 0.04$ , consider a transition from a state  $S = 7$  to the state  $S = 0$ , and calculate by how many metres we could lift a 1 kg weight if that “energy” difference could be converted into mechanical energy.

These differences do not stop us from using mathematical techniques common to the two models to our advantage.

## 2.2 The problem: bimodality, bistability, non-ergodicity

We first show how the bistability problem subtly appears with a set of experimental data, then explore its significance for larger population sizes.

### 2.2.1 Example with experimental data

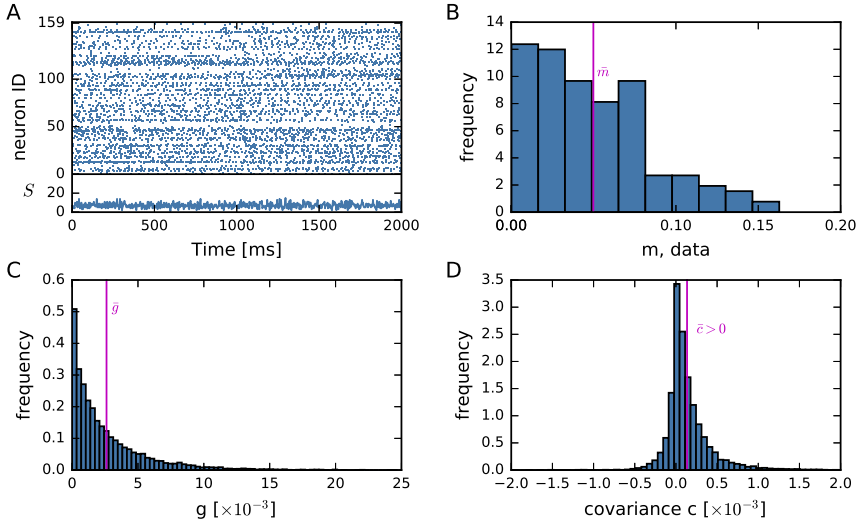
Our data consists in the activity of a population of 159 neurons ( $N = 159$ ) from motor cortex of macaque monkey, recorded for 15 minutes using a 100-electrode “Utah” array. See [164] for the experimental setup. The monkey was in a so-called “state of ongoing activity” [1], i.e. sitting on a chair without performing any task.

Figure 1A shows a two-second raster plot of the activity  $\mathbf{s}(t)$  of the recorded neurons. The time-varying population-summed activity  $S(t)$  is shown underneath. The time-averaged single and coupled activities  $m_i$ ,  $g_{ij}$ , and corresponding empirical covariances  $c_{ij}$  from the data are shown in panels B, C, D. The population averages of these quantities are

$$\bar{m} \approx 0.0499, \quad \bar{g} \approx 0.00261, \quad \bar{c} \approx 0.000135, \quad \bar{\rho} \approx 0.00319. \quad (18)$$

Let us find, via Boltzmann learning, the Lagrange multipliers of the pairwise maximum-entropy model constrained by the single and coupled activities plotted in fig. 1B–C. At each iteration, the sampling phase of the Boltzmann learning has  $10^6$  timesteps; an example is shown in fig. 2A. Note that the number of timesteps exceeds the ones used in Roudi et al. [52] ( $N = 200$ ) by a factor of ten and that in Broderick et al. [72] ( $N = 40$ ) by a factor of three. The learning converges and we obtain the Lagrange multipliers  $(\mu_i, \Lambda_{ij})$  whose distributions are shown in fig. 2D. The final single and coupled activities are shown in fig. 2C: they appear very close to the experimental ones. Sampling once more the maximum-entropy distribution with the obtained Lagrange multipliers, we obtain the population-average probability distribution, shown in fig. 2B against the empirical one. The tails of the two distributions differ, but this does not concern us now.

The results of the Boltzmann learning do not show any inconsistency at this point.



**Figure 1: Experimental data and their empirical first- and second-order statistics.** (A) Dot display of 159 parallel spike recordings of macaque monkey during a state of “ongoing activity”. The experimental data are recorded with a 100-electrode “Utah” array (Blackrock Microsystems, Salt Lake City, UT, USA) with 400  $\mu\text{m}$  interelectrode distance, covering an area of  $4 \times 4$  mm (subsession: s131214-002). The population-summed activity  $S(t)$  is the sum of the number of active neurons within time bin  $t$ . The time bins have width  $\Delta = 3$  ms. (B) Population distribution of the time-averaged activities  $m_i$ , eq. (4). The vertical line marks the population average,  $\bar{m} := \frac{1}{N} \sum_i m_i$ . (C) Population distribution of the time-averaged coupled activities  $g_{ij}$ , eq. (5). The vertical line marks the population average,  $\bar{g} := \frac{2}{N(N-1)} \sum_{i < j} g_{ij}$ . (D) Population distribution of the covariances  $c_{ij} = g_{ij} - m_i m_j$ . The vertical line again marks the population average,  $\bar{c} := \frac{2}{N(N-1)} \sum_{i < j} c_{ij}$ ; we have positive average correlations,  $\bar{c} > 0$ . (Histograms bins in B, C, D computed with Knuth’s rule [165]). Data courtesy of A. Riehle and T. Brochier.

But now we sample the distribution for a much longer time, say  $5 \times 10^7$  steps. fig. 3A shows what happens in a real instance. After roughly  $2 \times 10^6$  steps, the population jumps to a high-activity regime and remains there till the end of the sampling. We have discovered that the Glauber dynamics has an additional metastable high-activity regime. How many metastable regimes could there be? Starting the dynamics from states having different population-averages, we see that there are two metastable regimes; see fig. 3B. This means that the actual distribution associated with the Lagrange multipliers of fig. 2D must be *bimodal*.

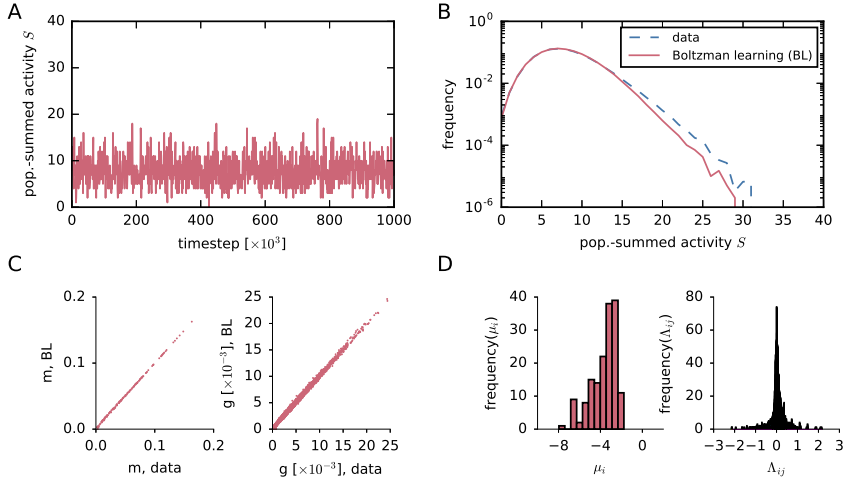


**Figure 2: Results of Boltzmann learning.** (A) Population-summed activity  $S(t)$  of  $N = 159$  neurons, obtained via Glauber dynamics in  $10^6$  timesteps. The couplings  $\Lambda_{ij}$  and biases  $\mu_i$  of the Glauber dynamics are the Lagrange multipliers, shown in panel D, found by Boltzmann learning from the experimental time-averages  $m_i$  and  $g_{ij}$  of fig. 1. (B) Red, solid: Probability distribution of the population-summed activity, sampled via the Glauber dynamics of panel A. Blue, dashed: empirical distribution of the population-summed activity from our dataset. (C) Time averages  $m_i$  and  $g_{ij}$  obtained from Boltzmann learning, versus experimental ones. (D) Population distribution of the Lagrange multipliers  $\mu_i$  and  $\Lambda_{ij}$  obtained via Boltzmann learning. (Histogram bins in D computed with Knuth’s rule [165]).

The discovery of the second metastable regime has important implications and causes quite a few problems:

- Our Boltzmann learning had actually not yet converged: if we sample long enough to allow the exploration of both metastable regimes, we find different time-averages of the single and coupled activities from those of fig. 2C, in complete disagreement with the experimental ones.
- The Lagrange multipliers we obtained, fig. 2D, are therefore not correct. Hence *the probability distribution obtained from the initial Boltzmann learning is not the true pairwise maximum-entropy distribution.*
- In order to sample the probability distribution around both modes and estimate their relative heights, we would need to observe many jumps between the two metastable regimes. The time required to observe one

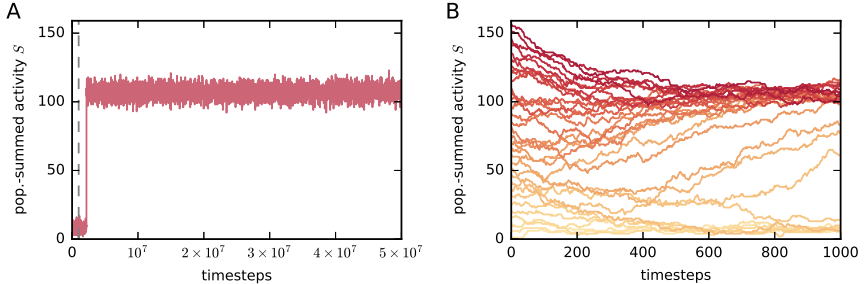


**Figure 3: Longer sampling: bistability.** (A) Population-summed activity  $S(t)$  obtained via Glauber dynamics, as in fig. 2A, but with longer sampling:  $5 \times 10^7$  timesteps. The dashed grey line marks the end of the previous sampling of fig. 2A. (B) Population-summed activities  $S(t)$  obtained from several instances of Glauber dynamics. Each instance starts with a different initial population activity  $s(0)$ , having different initial population sum  $S(0)$ , and is represented by a different red shade, from  $S(0) = 0$  (light red) to  $S(0) = N$  (dark red).

such jump seems to be larger than  $5 \times 10^7$  timesteps (we did not wait for longer), which is impractically long. For practical purposes the Glauber dynamics is *non-ergodic*, and the Boltzmann learning cannot proceed: *we cannot find the true pairwise distribution* within reasonable times.

- The Sessak-Monasson approximation [77, 78] is not correct either, because it gives a solution very close to the erroneous Boltzmann-learning one; the Lagrange multipliers of the sought-for maximum-entropy distribution evidently lie outside of its radius of convergence.

The reason why the initial result seemed self-consistent is that the sampling phase was too brief compared to the time needed to explore the full distribution: the latter time is so long that the dynamics is *non-ergodic* for computational purposes. This non-ergodicity effectively truncates the sampling at states  $\mathbf{s}$  for which  $\bar{s} \lesssim \theta$ , where  $\theta$  is the population-averaged activity at the trough between the two metastable regimes. In other words, the Lagrange multipliers  $\boldsymbol{\mu}, \boldsymbol{\Lambda}$  that we found belong to the “truncated” distribution

$$P_t(\mathbf{s} | \boldsymbol{\mu}, \boldsymbol{\Lambda}, \theta) \propto \begin{cases} \exp(\sum_i \mu_i s_i + \sum_{i < j} \Lambda_{ij} s_i s_j), & \bar{s} \leq \theta, \\ 0, & \bar{s} > \theta, \end{cases} \quad (19)$$

which is *not* a pairwise maximum-entropy distribution. The expectations of the single and coupled activities with respect to this distribution equal the experimental time averages:

$$\mathbb{E}_t(s_i) = m_i, \quad \mathbb{E}_t(s_i s_j) = g_{ij}, \quad (20)$$

but, again, these expectations do *not* come from the true pairwise maximum-entropy distribution, whose Lagrange multipliers remain unknown.

Everything is self-consistent as long as we use the truncated distribution  $P_t$ , but this is not the pairwise one  $P_p$ . This remark will be important later on.

Now the question is whether the correct, sought-for maximum-entropy distribution is also bimodal, or the Boltzmann learning simply encountered a bimodal distribution during its search of the correct one in the space of probabilities.

We make an educated guess by examining the analytically tractable reduced maximum-entropy model  $P_r$ , eq. (12). Using the population-averaged single and coupled activities as constraints,  $\mathbb{E}_r(\bar{s}_i) = \bar{m}$  and  $\mathbb{E}_r(\bar{s}_i \bar{s}_j) = \bar{g}$  from eq. (18), we numerically find the Lagrange multipliers of the reduced model:

$$\mu_r \approx -3.259, \quad A_r \approx 0.03859. \quad (21)$$

Note that in this case there is no sampling involved – the distribution can be calculated analytically – so the values above are correct within the numerical precision of the maximization procedure (interior-point method [59, chap. 10]). The values of the expected single and couple activities, re-obtained by explicit summation (not sampling) from the corresponding reduced maximum-entropy distribution, agree with the values eq. (18) to seven significant figures.

The resulting reduced maximum-entropy distribution for the population-summed activity,  $P_r(S|\mu_r, A_r)$ , is shown in fig. 4A, together with the experimental time-frequency distribution of our data. It shows a second maximum at roughly 90% activity. An exact analysis of small-population cases, and an analysis of large-population cases with a maximum-entropy model constrained by the population variance of the second moments, corresponding to constraining  $\mathbb{E}(S)$ ,  $\mathbb{E}(S^2)$ ,  $\mathbb{E}\left(\frac{S(S-1)}{N(N-1)} - \left(\frac{S(S-1)}{N(N-1)}\right)^2\right)$  (neither analysis is

discussed here), show that if a reduced maximum-entropy model is bimodal, the full inhomogeneous model is also bimodal, with a heightened second mode shifted towards lower activities with respect to the reduced model.

We therefore expect the correct, full pairwise maximum-entropy distribution for our data to be bimodal.

We will shortly propose a solution to the eliminate the bimodality. The basic idea behind this solution is easily grasped by first presenting an intuitive picture of how the bimodality arises.

### 2.2.2 Intuitive understanding of the bimodality: Glauber dynamics and mean-field picture

From the point of view of a network with couplings  $\mathbf{A}$  and biases  $\boldsymbol{\mu}$  whose evolution is described by a Glauber dynamics, the bimodality and associated bistability appear because the couplings  $\mathbf{A}$  are positive on average and symmetric, making the network an excitatory one.

The positivity of the couplings appears because the average correlation  $\bar{c}$  between neurons is positive (fig. 1D). But the symmetry of the couplings is also an essential factor. Consider a neuron  $i$  that on average projects negative couplings:  $\sum_{j \neq i} A_{ji} < 0$ . Such a neuron is “inhibitory on average” because its activation will on average inhibit the neurons it is coupled to. But, owing to coupling symmetry, “inhibitory on average” neurons are themselves inhibited on average, not excited. Self-regulatory feedback loops, possible in networks with asymmetric couplings, are impossible in this case, and excitation can lead to regimes with a higher activity. This phenomenon agrees with the known role of inhibitory neurons in controlling low irregular activity in inhibition-dominated regimes [166].

A naive mean-field analysis also confirms this. In the naive mean-field approximation we imagine that each neuron is coupled to a field representing the mean activities of all other neurons [73][74, ch. 4][167, ch. 6] (from the point of view of entropy maximization, we are replacing the maximum-entropy distribution with one representing independent activities, having minimal Kullback-Leibler divergence from the original one [168–170, chs 2, 16, 17]). Given the couplings  $\mathbf{A}$  and biases  $\boldsymbol{\mu}$ , the mean activities  $\mathbf{m}$  must satisfy  $N$

self-consistency equations

$$\tanh\left(\sum_{j \neq i} A_{ij} m_j + \mu_i\right) = m_i. \quad (22)$$

In the homogeneous case they reduce to the equation  $\tanh[(N-1)A_r \bar{m} + \mu_r] = \bar{m}$  and correspond to the intersection of two functions of  $\bar{m}$ : the line  $\bar{m} \mapsto \bar{m}$ , and the curve  $\bar{m} \mapsto \tanh[(N-1)A_r \bar{m} + \mu_r]$  that depends parametrically on  $(\mu_r, A_r)$ . See fig. 4D: for the Lagrange multipliers of our data, the curves these curves intersect at two different values of  $\bar{m}$ , meaning that there are two solutions to the self-consistency equation, corresponding to two different mean activities. These approximately correspond to the maxima of the probability distribution for the population average in fig. 4A.

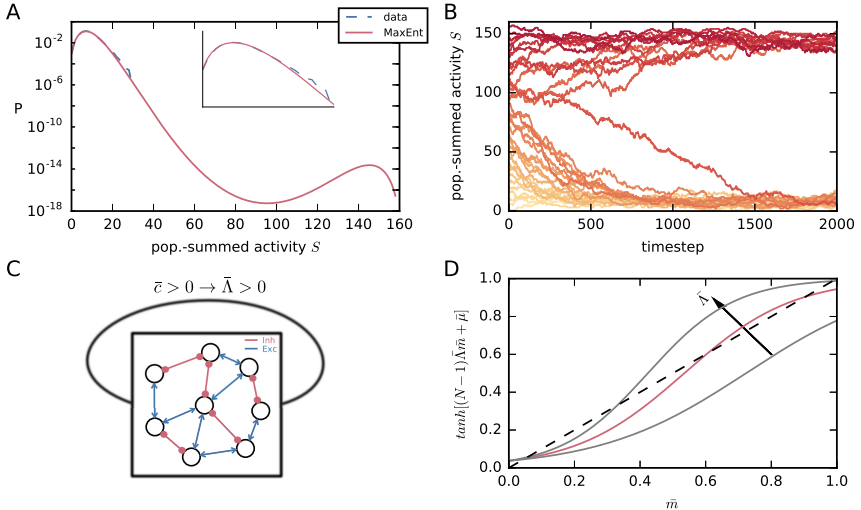


**Figure 4: Reduced maximum-entropy model and mean-field picture.** (A) Red, solid: Probability distribution for the population-summed activity,  $P_r(S)$  given by the reduced model for our dataset eq. (18); note the two probability maxima. Blue, dashed: empirical distribution of the population-summed activity from our dataset. (B) Population-summed activities  $S(t)$  obtained from several instances of Glauber dynamics associated with the reduced model, with homogeneous couplings,  $\Lambda_{ij} = \Lambda_r$ , and biases,  $\mu_i = \mu_r$ , of eq. (21). As in fig. 3, each instance starts with a different initial population activity  $s(0)$ , having different initial population sum  $S(0)$ , and is represented by a different red shade, from  $S(0) = 0$  (light red) to  $S(0) = N$  (dark red). (C) Illustration of a self-coupled symmetric network that is self-excitatory on average. Arrow-headed blue lines ( $\rightarrow$ ) represent excitatory couplings; circle-headed red lines ( $-\circ$ ) represent inhibitory couplings. (D) Self-consistency solution of the naive mean-field equation, illustrated for different  $\Lambda_r$ . Larger  $\Lambda_r$  causes two additional intersections, corresponding to one additional unstable and one additional stable solution. The red curve corresponds to the  $\Lambda_r$  calculated from our experimental data eq. (21).

### 2.2.3 Bistability ranges and population size

Is the appearance of bimodality peculiar to our experimental dataset, or can it be expected in other experimental datasets of neuronal activities? Will it disappear at larger neuronal populations, or will it become more prominent? We need to answer these questions to see whether this is a general problem.

We again make an educated guess using reduced maximum-entropy model and the distribution  $P_r(\bar{s}|\mu_r, \Lambda_r)$ , eq. (14). An elementary study of its convexity properties (second derivative) shows that this distribution can have one minimum in the interior,  $0 < \bar{s} < 1$ , or none, depending on the values of the parameters  $(\mu_r, \Lambda_r)$ . The distribution has two probability maxima if it has one such minimum for some value  $\bar{s}_m$ ,  $0 < \bar{s}_m < 1$ . The conditions for this are

$$\left. \frac{dP_r(\bar{s}|\mu_r, \Lambda_r)}{d\bar{s}} \right|_{\bar{s}=\bar{s}_m} = 0, \quad \left. \frac{d^2P_r(\bar{s}|\mu_r, \Lambda_r)}{d\bar{s}^2} \right|_{\bar{s}=\bar{s}_m} > 0, \quad 0 < \bar{s}_m < 1, \quad (23)$$

These conditions can be solved analytically and give the critical ranges of multipliers  $(\mu_r, \Lambda_r)$  for which bimodality occurs, parametrically in  $(\bar{s}_m, \Lambda_r)$ :

$$\left\{ \begin{array}{l} 0 < \bar{s}_m < 1, \\ \Lambda_r > \Psi'[1 + (1 - \bar{s}_m)N] + \Psi'(1 + \bar{s}_m N), \\ \mu_r(\bar{s}_m, \Lambda_r) = \Lambda_r/2 - \bar{s}_m N \Lambda_r - \Psi[1 + (1 - \bar{s}_m)N] + \Psi(1 + \bar{s}_m N), \end{array} \right. \quad (24)$$

where  $\Psi(x) := d \ln \Gamma(x)/dx$  and  $\Gamma$  is the Gamma function [171, ch. 6][172, chs 43, 44]. We then express the population-averaged single activity  $E_r(\bar{s})$  and Pearson correlation  $\bar{\rho}$ , typically used in the literature, in terms of  $(\mu_r, \Lambda_r)$  using the definitions eq. (17) and the probability eq. (14). Finally we obtain the bimodality range for  $(E_r(\bar{s}), \bar{\rho})$ , parametrically in  $(\bar{s}_m, \Lambda_r)$  within the bounds eq. (24).

The result is shown in fig. 5A for various values of  $N$ . A curve is associated with each  $N$ ; values of  $(E_r(\bar{s}), \bar{\rho})$  above such curves yield a bimodal distribution in the homogeneous case.

Most important, fig. 5A shows that the maximum-entropy distribution will be bimodal for larger ranges of mean activities and correlations, as the population size  $N$  increases. Empirical population-averaged quantities, on the other hand, should not change with population size if they are sampled from a biologically homogeneous neural population. This means that even if maximum-entropy does not predict a bimodal distribution for the measured activities and correlations of a particular small sample, it will predict a bimodal distribution for a larger sample in a similar experimental setup. This phenomenon is shown in fig. 5B: keeping our constraints eq. (18) fixed, when  $N \lesssim 150$  the distribution has only one maximum for low activity,

$\bar{s} \approx 0.0497$ , and when  $N \gtrsim 150$  a second probability maximum for high activity,  $\bar{s} \approx 0.9502$ , appears. The probability at this second maximum increases sharply until  $N \approx 200$  and thereafter maintains an approximately stable value, roughly 6000 times smaller than the low-activity maximum. The minimum between the two modes becomes deeper and deeper as we increase  $N$  above 200.

As mentioned in the previous section, exact studies with small samples and studies with large samples and a different reduced model, which takes into account the population-variance of the second moments, indicate that the high-activity maximum in the inhomogeneous case is larger (roughly 2000 times smaller than the low-activity one when  $N = 1000$ ) and shifted towards lower activities ( $\bar{s} \approx 0.25$  when  $N = 1000$ ).

This can also be seen by adding a Gaussian jitter to the multipliers of the reduced case  $\mu_i = \mu_r$ ,  $A_{ij} = A_r$ , making it inhomogeneous. The results are shown in fig. 5C–D. The basin of attraction of the second metastable regime is shifted to lower activities, and transitions between the two metastable regimes become more likely for larger jitters. This means that inhomogeneity makes the minimum in between the two modes shallower. The obtained distribution is mathematically identical with the Boltzmann distribution of the Sherrington & Kirkpatrick infinite-range spin-glass [142, 143]. A more systematic analysis of the effect of inhomogeneity could therefore employ methods developed for spin glasses [173].

The population-averaged activity and Pearson correlation of our data (violet “3 ms” point in fig. 5A) fall within the bimodality range, as expected. The important question is whether our dataset is a typical representative of this bimodality problem, or an outlier. It is not an easy question to answer, as this kind of experimental data are still rare, but we take as reference the data summarized in Table 1 of Cohen & Kohn [44], which reports firing rates and spike-count correlations  $r_{SC}$ . The reported firing rates correspond to population-averaged activities  $\bar{m}$  ranging between 0.02 and 0.25, if we use 3 ms time-bins. We only need to estimate our Pearson correlation  $\rho$  from their spike-count correlation  $r_{SC}$ . Both are particular cases of the “cross-

correlogram metric”  $r_{\text{CCG}}$  introduced by Bair et al. [174, App. A]:

$$r_{\text{CCG } ij}(\tau) := \frac{\mathbb{E}(\nu_i(\tau)\nu_j(\tau)) - \mathbb{E}(\nu_i(\tau))\mathbb{E}(\nu_j(\tau))}{\sqrt{[\mathbb{E}(\nu_i(\tau)^2) - \mathbb{E}(\nu_i(\tau))^2][\mathbb{E}(\nu_j(\tau)^2) - \mathbb{E}(\nu_j(\tau))^2]}}, \quad (25)$$

with  $\nu_i(\tau) := \sum_{t=1}^{\tau} s_i(t)$ ,

i.e.  $\nu_i(\tau)$  is the number of spikes of neuron  $i$  during the (real-)time window  $\tau\Delta$ . This metric also equals the area between times  $-\tau\Delta$  and  $\tau\Delta$  under the cross-correlogram of neurons  $i$  and  $j$  (stationarity is assumed). The spike count correlation  $r_{\text{SC}}$  corresponds to  $\tau = n \equiv T/\Delta$ , and our Pearson correlation  $\rho$  to  $\tau = 1$ . Several studies [174–178] report either measured values of  $r_{\text{CCG}}(\tau)$  for different windows  $\tau$ , or measured cross-correlograms. From their analysis we can approximately say that  $\rho \lesssim r_{\text{SC}}/20$ , so we take  $\bar{\rho} = \overline{r_{\text{SC}}}/20$  as a safest-case value (i.e. as far away from bimodality as possible).

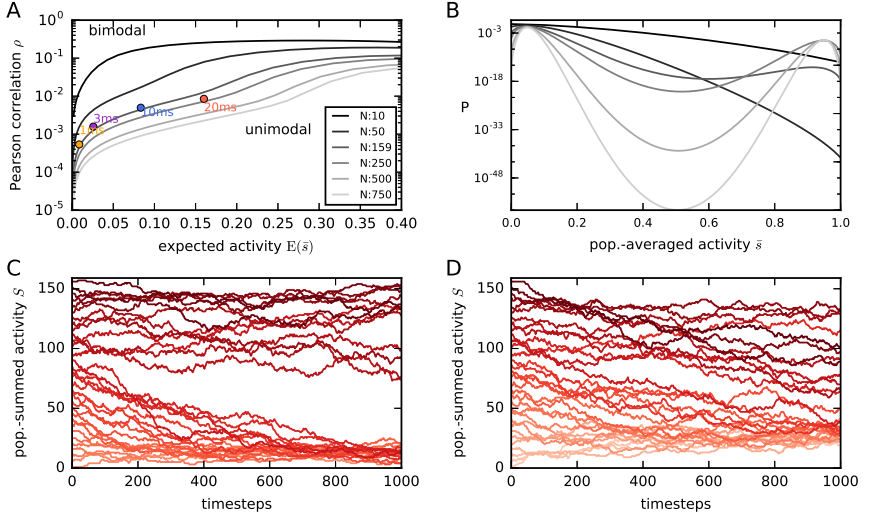


**Figure 5: Bimodality ranges for the reduced model and effects of inhomogeneity.** (A) The reduced maximum-entropy model eq. (12) yields a distribution  $P_r(\bar{s})$  that is either unimodal or bimodal, depending on the number of neurons  $N$  and the values of the experimental constraints  $(E_r(\bar{s}), \bar{\rho})$ . Each curve in the plot corresponds to a particular  $N$  (see legend) and separates the values  $(E_r(\bar{s}), \bar{\rho})$  yielding a unimodal distribution (below the curve) from those yielding a bimodal one (above the curve). The curves are symmetric with respect to  $E_r(\bar{s}) = 0.5$  (ranges  $E_r(\bar{s}) > 0.4$  not shown). Note how the range of constraints yielding bimodality increases with  $N$ . Coloured dots show the experimental constraints for our dataset, for different time-binnings with widths  $\Delta = 1$  ms,  $\Delta = 3$  ms,  $\Delta = 10$  ms,  $\Delta = 20$  ms. (B) Probability distributions of the reduced model for the population-summed activity,  $P_r(S|N)$ , obtained keeping the constraints eq. (18) fixed and using different  $N$  (same legend as panel A). (C) Population-summed activities  $S(t)$  from several instances of Glauber dynamics, all with the same normally-distributed couplings  $\Lambda_{ij}$  and biases  $\mu_i$ , with means as in eq. (21) and fig. 4B, and standard deviations  $\sigma(\Lambda_{ij}) = 0.009$ ,  $\sigma(\mu_i) = 0.8$ . Each instance starts with a different initial population activity  $s(0)$ , having different initial population sum  $S(0)$ , and is represented by a different red shade, from  $S(0) = 0$  (light red) to  $S(0) = N$  (dark red). Note how the basins of attraction of the two metastable regimes are wider than in the homogeneous case of fig. 4B. (D) The same as panel C, but with larger standard deviations  $\sigma(\Lambda_{ij}) = 0.019$ ,  $\sigma(\mu_i) = 1.6$ ; the jumps between the two metastable regimes become more frequent than in fig. 4B, indicating that the minimum between the modes becomes more shallow with increasing inhomogeneity.

Under these approximations the greatest part of the values summarized by Cohen & Kohn fall in the bimodality regions of fig. 5A if  $N = 250$ , and almost

all of them if  $N = 500$ ; see fig. 6. These data points have only an indicative value but suggest that our dataset is not an outlier for the bimodality problem. If those data had been recorded from a population of 500 neurons, they would have yielded a bimodal pairwise maximum-entropy model. The bimodality problem and its consequences need to be taken seriously. Is there any way to eliminate it?

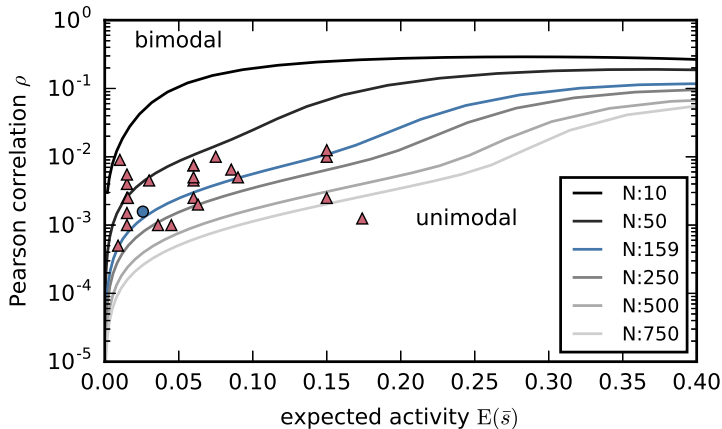


**Figure 6: Bimodality for experimental data from neuroscientific literature.** Mean activities and correlations  $(E_r(\bar{s}), \bar{\rho})$  inferred from experimental data reported in Cohen & Kohn [44, Table 1], plotted upon the curves separating bimodal from unimodal maximum-entropy distributions of fig. 5A. The plot suggests that typical experimental neural recordings of 250 neurons and above are likely to lead to bimodal maximum-entropy pairwise distributions.

### 2.3 Eliminating the bimodality: an inhibited maximum-entropy model and Glauber dynamics

We already mentioned in the Introduction why a maximum-entropy model yielding a bimodal distribution in the population-summed activity is problematic:

- The presence of two sharply distinct modes does not seem realistic in view of present neuroscientific data, so the model is making unrealistic

predictions. The situation is even worse if the second mode peaks at 90% – 90 neurons out of 100 simultaneously active!

- As  $N$  increases, the second mode becomes more pronounced, and the minimum between the modes shallower: above a particular population size, the bimodality cannot be dismissed as a small mathematical quirk.
- The Boltzmann-learning procedure based on Glauber dynamics becomes practically non-ergodic and the Lagrange multipliers of the model are difficult or impossible to find.
- The Glauber dynamics based on the pairwise model jumps between two metastable regimes and cannot be used to generate realistic surrogate data.
- Finally, the fact that the position and height of the second mode depend on  $N$  (in the inhomogeneous case) goes against basic statistical expectations. If we consider the  $N$  neurons to be a sample, chosen in an unsystematic way, of a larger population, then the maxima in our probability assignments for the population averages of the sample and of the larger population should roughly coincide (the former being obtained from the latter by convolution with a hypergeometric distribution).

We now propose a way to eliminate the bimodality and the above problems. Let us re-examine what happens with the Glauber dynamics first.

### 2.3.1 Importance of inhibition in neural networks: modified Glauber dynamics

As mentioned in Intuitive understanding of the bimodality: Glauber dynamics and mean-field picture, from the Glauber-dynamical viewpoint jumps to high activities happen because the couplings  $\mathbf{A}$  are positive on average and symmetric, making the network an excitatory one.

The positivity of the couplings is inevitable: it corresponds to an experimentally observed positive average correlation. Their symmetry, on the other hand, is a mathematical feature of the pairwise model – and, if we made an ungranted parallel with synaptic couplings, it would not be a realistic feature.

Can we try to break this symmetry somehow? Can we add a minimal amount of asymmetric inhibition to the Glauber dynamics?

The answer is yes, in a very simple way: by connecting all  $N$  neurons to a single inhibitory neuron that instantaneously activates whenever their average activity exceeds a threshold  $\theta$ , having a value in the set  $\{1/N, 2/N, \dots, (N-1)/N\}$  (the cases  $\theta = 0$  or  $1$  are trivial). Upon activation, the inhibitory neuron sends inhibitory feedback,  $A_I < 0$ , to all other  $N$  neurons (see fig. 7A). The algorithm for this “inhibited” Glauber dynamics (including how the “instantaneously” is implemented) is explained in the Materials and Methods section.

The results from simulations of the inhibited Glauber dynamics are shown in fig. 7C–D; in all cases the inhibitory coupling  $A_I = -24.7$  and the inhibition threshold  $\theta = 0.3$ . In the reduced homogeneous case the couplings  $A_{ij} = A_r$  and biases  $\mu_i = \mu_r$ , eq. (21), are the same that led to bistability in fig. 4B; in the inhomogeneous case they are the same, normally distributed, that led to bistability in fig. 5C–D. In either case, the additional inhibitory neuron has eliminated the bistability, leaving only the stable low-activity regime.

Furthermore, also in the case of the inhomogeneous couplings and biases (distributed as in fig. 2D) that caused the quasi-non-ergodic behaviour in our first Boltzmann learning results, fig. 3, the addition of the inhibitory neuron (again with  $A_I = -24.7$ ,  $\theta = 0.3$ ) eliminates the second metastable state: see fig. 7E.

In summary: the asymmetric coupling of an additional inhibitory neuron clearly eliminates the bistability of the Glauber dynamics. This works for any network size  $N$  with an appropriate choice of the inhibitory coupling  $A_I < 0$  and threshold  $\theta$ .

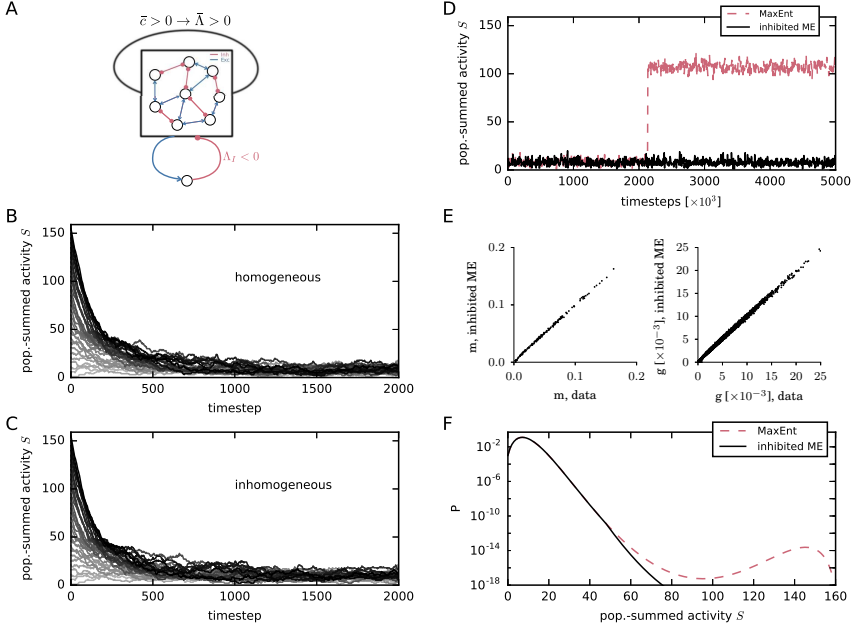


**Figure 7: Asymmetric inhibition and elimination of bimodality and non-ergodicity.** (A) Illustration of self-coupled network with additional asymmetric inhibitory feedback. Each neuron receives inhibitory input  $\lambda_I < 0$  from the additional neuron whenever the population-average  $\bar{s}$  becomes greater than the inhibition threshold  $\theta$ . (B) Population-summed activities  $S(t)$  from several instances of the inhibited Glauber dynamics, with  $\lambda_I = -25$ ,  $\theta = 0.3$ , and same homogeneous  $\lambda_{ij} = \lambda_r$ ,  $\mu_i = \mu_r$  of eq. (21), as used for fig. 4B. Each instance starts with a different initial population activity  $s(0)$ , having different initial population sum  $S(0)$ , and is represented by a different grey shade, from  $S(0) = 0$  (light grey) to  $S(0) = N$  (black). Note the disappearance, thanks to inhibition, of the bistability that was evident in the “uninhibited” case of fig. 4B. (C) Analogous to panel B, with  $\lambda_I = -25$ ,  $\theta = 0.3$ , but inhomogeneous normally distributed couplings and biases as in the uninhibited case of fig. 5C. Note again the disappearance, thanks to inhibition, of the bistability that was evident in the activities  $S(t)$  of that figure. (D) Comparison of a longer ( $5 \times 10^6$  timesteps) Glauber sampling with couplings and biases of fig. 2D obtained from our first Boltzmann learning, and inhibited-Glauber sampling with same couplings and biases and  $\lambda_I = -25$ ,  $\theta = 0.3$ . The comparison confirms that inhibition eliminates the second metastable regime and makes the Glauber dynamics ergodic. (E) Time averages  $m_i$  and  $g_{ij}$  obtained from Boltzmann learning for the inhibited model  $P_i$ , versus experimental ones. (F) Probability distribution of the population-summed activity  $P_i(S)$  given by the inhibited model eq. (26) for our dataset eq. (18), compared with the one previously given by the reduced model  $P_r(S)$ , fig. 4A. Asymmetric inhibition, expressed by the reference prior eq. (29), has eliminated the second mode.

We now show that this idea also eliminates our original problem: the bimodality of the pairwise maximum-entropy model.

### 2.3.2 Inhibited maximum-entropy model

The pairwise maximum-entropy model is the stationary distribution of the Glauber dynamics with symmetric couplings. We have now modified the latter in an asymmetric way. The stationary distribution of the inhibited Glauber dynamics of fig. 7 cannot, therefore, be a pairwise maximum-entropy model. It turns out, however, that *it is still a maximum-entropy model*, of the following form:

$$P_i(\mathbf{s} | \boldsymbol{\mu}, \mathbf{A}, \Lambda_I, \theta) = \frac{1}{Z_i(\boldsymbol{\mu}, \mathbf{A}, \Lambda_I, \theta)} \times \exp \left[ \sum_i \mu_i s_i + \sum_{i>j} \Lambda_{ij} s_i s_j + \Lambda_I N G(\bar{s} - \theta) \right], \quad (26)$$

$$Z_i(\boldsymbol{\mu}, \mathbf{A}, \Lambda_I, \theta) := \sum_{\mathbf{s}} \exp \left[ \sum_i \mu_i s_i + \sum_{i>j} \Lambda_{ij} s_i s_j + \Lambda_I N G(\bar{s} - \theta) \right],$$

$$G(\bar{s} - \theta) := (\bar{s} - \theta) H(\bar{s} - \theta),$$

where  $\Lambda_I$  is the (negative, in our case) coupling strength from the inhibitory neuron to the other neurons,  $\theta$  is the activation threshold of the inhibitory neuron, and  $H$  is the Heaviside step function. We call eq. (26) the *inhibited pairwise maximum-entropy model*.

The function  $G(\bar{s} - \theta)$  (plotted in fig. 8 together with its exponential) can also be written as a linear combination of population-averaged  $K$ -tuple activities,  $s_{i_1} s_{i_2} \cdots s_{i_K}$ , for  $K$  equal to  $N\theta$  and larger (we leave the proof of this as a classic “exercise for the reader”):

$$N G(\bar{s} - \theta) = \sum_{K=N\theta}^N \binom{-N\theta}{-K+1} \left( \sum_{i_1 < i_2 < \cdots < i_K} s_{i_1} s_{i_2} \cdots s_{i_K} \right), \quad (27)$$

the linear coefficients being binomial coefficient functions [179], which have alternating signs. For example, if  $N = 5$  and  $\theta = 3/5$ ,

$$N G(\bar{s} - \theta) = (s_2 s_3 s_4 s_5 + s_1 s_3 s_4 s_5 + s_1 s_2 s_4 s_5 + s_1 s_2 s_3 s_5 + s_1 s_2 s_3 s_4) - 3 s_1 s_2 s_3 s_4 s_5. \quad (28)$$

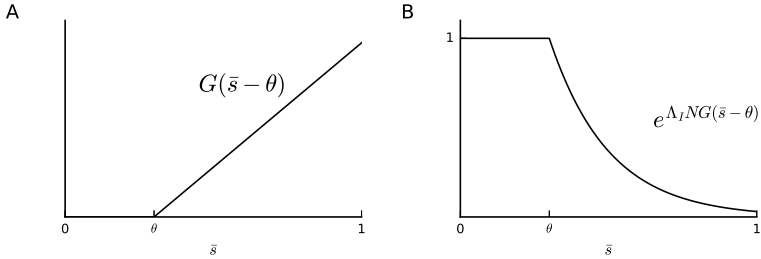


**Figure 8: Reference prior.** The function  $G(\bar{s} - \theta)$  and its exponential

(This function differs from the additional function appearing in maximum-entropy model by Tkačik et al. [88, 180, 181], which consists in  $N + 1$  constraints enforcing the observed population-average distribution. For reasons discussed at the end of § 2.1.1, the use of all those constraints may not be justified or meaningful.)

The stationarity of the distribution  $P_i(\mathbf{s})$  under the inhibited Glauber dynamics is proved in the Materials and Methods section. This distribution is a maximum-entropy model in two different ways:

- (a) As an application of the minimum-relative-entropy (minimum-discrimination-information) principle [24, 28, 34, 91–102], with the pairwise constraints eq. (8), with respect to the reference (or prior) probability distribution

$$P_0(\mathbf{s} | \Lambda_I, \theta) \propto \exp[\Lambda_I N G(\bar{s} - \theta)], \quad (N\theta \in \{1, 2, \dots, N - 1\}). \quad (29)$$

This distribution assigns decreasing probabilities to states with average activities above  $\theta$ ; see fig. 8B. This probability can be interpreted as arising from a more detailed model in which we know that external inhibitory units make activities above the threshold  $\theta$  increasingly improbable (we explain this in the Discussion section). In this interpretation the parameters  $\Lambda_I$  and  $\theta$  are chosen a priori.

- (b) As an application of the “bare” maximum-entropy principle, given the pairwise constraints eq. (8) and an additional constraint for the

expectation of  $N G(\bar{s} - \theta)$ :

$$\begin{aligned} E_i(N G(\bar{s} - \theta)) &= \sum_{S=N\theta}^N (S - N\theta) P_i(S) \\ &= \sum_{K=N\theta}^N \binom{-N\theta}{-K+1} E_i \left( \sum_{i_1 < i_2 < \dots < i_K} s_{i_1} s_{i_2} \dots s_{i_K} \right). \end{aligned} \quad (30)$$

This is a constraint of the “tail first moment”, so to speak, of the probability for the population-averaged activity  $P_i(\bar{s})$ : it determines whether the right tail of  $P_i(\bar{s})$  has a small ( $\Lambda_I < 0$ ) or heavy ( $\Lambda_I > 0$ ) probability. It can also be seen as a constraint on the  $N\theta$ th and higher moments, owing to eq. (27). In this interpretation the parameter  $\Lambda_I$  is the Lagrange multiplier associated with this constraint, hence it is determined by the data; the parameter  $\theta$  is still chosen a priori. Note, however, that experimental data are likely to give a vanishing time average of  $N G(\bar{s} - \theta)$ , so that  $\Lambda_I = -\infty$ . This interpretation has therefore to be used with care, for the reasons discussed at the end of § 2.1.1.

The inhibited model  $P_i$  includes Shimazaki’s model [51] and its “simultaneous silence” constraint as the limit  $\Lambda_I \rightarrow -\infty$ ,  $\theta = 1/N$ . Because of this limit, Shimazaki’s model has a sharp jump in probability when  $\bar{s} = 1/N$  (the constraint uniformly removes probability from  $P(\bar{s} > 1/N)$  and gives it to  $P(\bar{s} = 0)$ ), whereas the inhibited model  $P_i$  only presents a kink when  $\bar{s} = \theta$ , with a discontinuity in the derivative proportional to  $\Lambda_I$ .

Several features of the inhibited maximum-entropy model eq. (26) are worth remarking upon:

1. The inhibited distribution  $P_i$  includes the pairwise one  $P_p$ , eq. (6), as the particular case  $\Lambda_I = 0$  (obviously, as this is equivalent to removing the inhibitory neuron).
2. Pairwise and inhibited distributions  $P_p$  and  $P_i$  having same Lagrange multipliers  $(\boldsymbol{\mu}, \boldsymbol{\Lambda})$  are *equal* if restricted to states with population-averaged activity below the threshold  $\theta$ , because  $G(\bar{s} - \theta) = 0$  if  $\bar{s} \leq \theta$ :

$$P_p(\mathbf{s} | \boldsymbol{\mu}, \boldsymbol{\Lambda}, \bar{s} \leq \theta) = P_i(\mathbf{s} | \boldsymbol{\mu}, \boldsymbol{\Lambda}, \Lambda_I, \theta, \bar{s} \leq \theta). \quad (31)$$

Said otherwise, the pairwise and inhibited distributions have the same shape for  $\bar{s} \leq \theta$ , modulo rescaling by a constant factor:

$$P_i(\mathbf{s} | \boldsymbol{\mu}, \boldsymbol{\Lambda}, \Lambda_I, \theta) = P_p(\mathbf{s} | \boldsymbol{\mu}, \boldsymbol{\Lambda}) \times \frac{Z_p(\boldsymbol{\mu}, \boldsymbol{\Lambda})}{Z_i(\boldsymbol{\mu}, \boldsymbol{\Lambda}, \Lambda_I, \theta)}, \quad \bar{s} \leq \theta. \quad (32)$$

3. For states with average activity  $\bar{s}$  above the threshold  $\theta$ , the inhibited model is a “squashed” version of the pairwise one when  $\Lambda_I < 0$ :

$$P_i(\mathbf{s} | \boldsymbol{\mu}, \boldsymbol{\Lambda}, \Lambda_I, \theta) \propto P_p(\mathbf{s} | \boldsymbol{\mu}, \boldsymbol{\Lambda}) \times \exp[N\Lambda_I(\bar{s} - \theta)], \quad \bar{s} > \theta. \quad (33)$$

4. If  $\Lambda_I \neq 0$ , then inhibited and pairwise models with the same Lagrange multipliers  $(\boldsymbol{\mu}, \boldsymbol{\Lambda})$  have *different* expectations for single and coupled activities:

$$\begin{aligned} E_i(s_i | \boldsymbol{\mu}, \boldsymbol{\Lambda}, \Lambda_I, \theta) &\neq E_p(s_i | \boldsymbol{\mu}, \boldsymbol{\Lambda}), \\ E_i(s_i s_j | \boldsymbol{\mu}, \boldsymbol{\Lambda}, \Lambda_I, \theta) &\neq E_p(s_i s_j | \boldsymbol{\mu}, \boldsymbol{\Lambda}), \end{aligned} \quad (34)$$

and obviously also different covariances and correlations.

Remarks 2 and 3 above imply that if the inhibitory coupling  $\Lambda_I$  is negative and very large, so that  $\exp[N\Lambda_I(\bar{s} - \theta)] \approx 0$  when  $\bar{s} > \theta$ , then *the inhibited maximum-entropy distribution  $P_i$  is approximately equal to the truncated distribution  $P_t$*  – the incorrect one eq. (19) obtained via Boltzmann learning – having the same multipliers  $(\boldsymbol{\mu}, \boldsymbol{\Lambda})$  and threshold  $\theta$ :

$$P_i(\mathbf{s} | \boldsymbol{\mu}, \boldsymbol{\Lambda}, \Lambda_I, \theta) \approx P_t(\mathbf{s} | \boldsymbol{\mu}, \boldsymbol{\Lambda}, \theta) \quad \text{if } \Lambda_I \ll -1, \quad (35)$$

(mathematically speaking we have pointwise convergence as  $\Lambda_I \rightarrow -\infty$ ), and their expectations are also approximately equal. This suggests a way to reinterpret and keep the results of our first Boltzmann-learning algorithm fig. 2.

### 2.3.3 Boltzmann learning for the inhibited maximum-entropy model

Our first Boltzmann-learning calculation, with results shown in fig. 2, returned a distribution that reproduced the desired constraints  $(\mathbf{m}, \mathbf{g})$ . But that distribution turned out to be not the true pairwise maximum-entropy one, but a truncated version of it  $P_t$ , eq. (19), owing to the bimodality of the true pairwise distribution and the resulting non-ergodicity.

If we had we decided to apply the inhibited pairwise maximum-entropy model  $P_i(\mathbf{s}|\boldsymbol{\mu}, \mathbf{A}, \Lambda_I, \theta)$  (with  $\Lambda_I \ll -1$  and  $0.3 \lesssim \theta \lesssim 0.5$ ) to our data, instead of the pairwise one  $P_p(\mathbf{s}|\boldsymbol{\mu}, \mathbf{A})$ , and had sought its Lagrange multipliers via Boltzmann learning, then the results would have been the same as in fig. 2. It is clear why: the inhibitory neuron would not have allowed jumps to higher activities, unlike fig. 3A (see fig. 7D); and at the same time it would not have influenced the dynamics below  $\bar{s} \approx 0.3$  (i.e.  $S \approx 50$ ). The sampling phase of our Boltzmann learning would have been sufficient. We confirm this by applying Boltzmann-learning procedure (with the inhibited Glauber dynamics) to find the multipliers of the inhibited model with  $\Lambda_I = -25$ ,  $\theta = 0.3$ . The resulting multipliers are close to those in fig. 2D, and the constraints are satisfied, see fig. 7E.

Results obtained with a non-ergodic Boltzmann learning, and therefore incorrect for the pairwise maximum-entropy model, can therefore be reinterpreted as correct results for the inhibited pairwise maximum entropy model, with appropriately chosen  $\Lambda_I$  and  $\theta$ . This is important for any work in the literature that may unknowingly have been affected by non-ergodicity.

### 3 Discussion

#### 3.1 Summary

The pairwise maximum-entropy model, applied to experimental neuronal data of populations of 200 and more neurons, is very likely to give a *bimodal* probability distribution for the population-averaged activity,  $P(\mathbf{s})$ . We have provided evidence for this claim in § 2.2, starting from an experimental dataset and then looking at summarized data from the literature. The first mode is the one observed in the data. The second mode (unobserved) can appear at very high activities (even 90% of the population simultaneously active) and its height increases with population size.

The presence of a second mode is problematic for several reasons:

- As far as we know, a second mode has never been observed in experimental recordings, and surely not at high activity – data in which 180 out of 200 neurons spike simultaneously are unheard of. So it is an unrealistic prediction of the pairwise model.

- Above certain population sizes the second mode cannot be dismissed as too small to be recorded, because it becomes more pronounced as  $N$  increases, and the minimum that separates it from the main mode becomes shallower.
- The Boltzmann-learning [70–72] procedure based on asynchronous Glauber dynamics [65, 69, chap. 29] becomes practically non-ergodic – it can already be so for population sizes of roughly 50 neurons – so that the Lagrange multipliers of the pairwise model are difficult or impossible to find. Approximate methods like mean-field [73–75], Thouless-Anderson-Palmer [75, 76], Sessak-Monasson [77, 78] also seem to break down in this case.
- The Glauber dynamics based on the pairwise model jumps between two metastable regimes, remaining in each for long times (owing to its asynchronous update) and cannot be used to generate realistic surrogate data.
- The fact that the position and height of the second mode vary with  $N$  contradicts the natural assumption that the recorded  $N$  neurons are a “random sample” of a larger population. (The probability calculus tells us that the population-average distributions of a full population and a “random sample” from it should have maxima at roughly the same relative heights and locations, since they are connected by convolution with a hypergeometric distribution [182, ch. II][183, ch. 4][38, ch. 3][cf. also 184–188].)

Eliminating the second mode also eliminates all these problems.

We gave an intuitive explanation of why the second mode appears: because the pairwise model, given positive pairwise correlations, corresponds to a network that is excitatory on average and symmetric. And symmetric connectivity is incompatible with the presence of a subset of neurons that have an inhibitory effect, but receive excitatory input (see § 2.2.2). This explanation also suggested a way to eliminate the second mode: by adding a minimal asymmetric inhibition to the network, in the guise of an additional, asymmetrically coupled inhibitory neuron (fig. 7A).

This idea led to the construction of an “inhibited” pairwise maximum-entropy model  $P_1(\mathbf{s})$ , eq. (26), with the important properties:

- It is a maximum-entropy or minimum-relative-entropy model.
- It is the stationary distribution of a particular asynchronous Glauber dynamics with pairwise couplings.
- Its Lagrange multipliers can be found via Boltzmann learning.
- Its parameters can be chosen to have the main mode only.
- It is numerically equal to the distribution one would obtain from a non-ergodic Boltzmann learning.

### 3.2 In defence of the inhibited model

We have already argued at length that bimodality is a problem in the application of the pairwise model, and do not dwell on this in this discussion. We wish to stress, though, that the presence of bimodality and non-ergodicity can easily go unnoticed. We urge researchers who use Boltzmann learning or one of the mentioned approximations to check for the presence of bimodality and non-ergodicity by starting the sampling from different initial conditions, at low and high activities, looking out for bistable regimes [cf. 66, § 2.1.3]. One way out of this problem is to use other sampling techniques or Markov chains different from the Glauber one [64–66, 189].

Different readers will draw different conclusions from the presence of bimodality. Some may dismiss or abandon the whole pairwise model as flawed. Some may still want to use it, bimodality notwithstanding. Some may look for other maximum-entropy-inspired alternatives. We have presented *one* (as opposed to *the*) such alternative: the “inhibited” pairwise maximum-entropy model  $P_1$ , eq. (26). It is an interesting alternative for at least two reasons.

First, the inhibited distribution  $P_1$  is stationary under a Glauber dynamics with *pairwise* couplings. Consider that pairwise models with additional constraints are stationary under Gibbs samplers with higher-order couplings – and thus lose some of their analogies with real neuronal networks.

Second, the inhibited distribution  $P_i$  incorporates the effects of neural inhibition in a simple way. These effects are represented by the reference or prior probability  $P_0(\mathbf{s} | A_I, \theta)$ , eq. (29).

Some readers may actually object to the usefulness of the inhibited distribution  $P_i$  exactly because it is derived from a particular prior via minimum-relative-entropy, and may thus appear less “non-committal” or less “unstructured” than a “bare” maximum-entropy one. We would like to briefly counter this argument by pointing out that bare maximum-entropy can be quite “committal”, and that reference priors can correct that.

The statement “the maximum-entropy method gives the maximally non-committal probability distribution consistent with the given information” and variations thereof are frequently repeated in the literature. But there are many qualifications behind this statement, especially behind the terms “non-committal” and “information”. The term “information” does not mean only “experimental data”: it also means knowledge of the *assumptions underlying* the specified problem and the variables implied. The way we set up a maximum-entropy problem implies many underlying assumptions, already before experimental data are taken into account [35, 190].

A concrete assumption underlying the bare maximum-entropy principle applied to neuronal activity is that *the recorded neurons are not a sample from a larger population of neurobiologically similar neurons*. It is easy to expose this assumption in the homogeneous case. If we assume that our  $N$  neurons are a sample from a larger population, the maximum-entropy principle requires that the moment constraints be applied to the average of the *full* population, not of the sample [188, § 3.2]. The marginal distribution of the sample will *not* be a maximum-entropy distribution. The assumption above is quite strong and neurobiologically unrealistic, but does not seem to have bothered researchers who applied maximum-entropy to samples; or maybe it escaped their attention. In any case it shows that the bare maximum-entropy principle is far from “non-committal” or “unstructured”.

The “committal” nature of bare maximum-entropy also appears in its derivation from the probability calculus. This derivation requires a particular prior [31, 34, 35, 115, 190], but one could use other, quite natural priors (e.g., the “flat prior over probability distributions” considered by Bayes [191,

Scholium] and Laplace [192, p. xvii]) and the result would *not* be a bare maximum-entropy distribution.

Reference priors can in some cases correct such implicit assumptions. For example, consider a pair of neurons with binary states  $s_1$  and  $s_2$ . Without “experimental data”, the maximum-entropy principle assigns a uniform probability of  $1/4$  to each of the four possible joint states  $(s_1, s_2)$ . The probability assigned to the total activity,  $S := s_1 + s_2$ , is therefore *not uniform* ( $2/4$  probability to  $S = 1$  and  $1/4$  probability to the remaining two values). If we apply the maximum-entropy principle to the total activity  $S$  directly, instead, it gives a *uniform* probability of  $1/3$ . Both applications of the principle are consistent, but they use different assumptions about the structure of the biophysical problem. The information implicit in the first application can be specified in the second by using the minimum-relative-entropy method with a non-uniform prior distribution assigning  $2/4$  probability to  $S = 1$ . (Something analogous happens in statistical mechanics with the probability distribution for energy, in which a “density of states” term multiplies the Boltzmann factor). Some implicit assumptions, however, like the sampling assumption previously discussed, cannot be corrected by reference priors.

The necessity of reference priors, reflecting deeper assumptions, is well-known in maximum-entropy image reconstruction [193, 194], for example of astronomical sources [194, 195]: as Skilling remarked, “bare maximum-entropy is surprised to find isolated stars, but astronomers are not” [35].

An analogous remark can be made in our case: bare maximum-entropy is surprised to find so many inactive neurons, and it tries to make some more active ones by creating a second maximum, if that does not break the constraints. But neuroscientists are not surprised at inactive neurons. Bare maximum-entropy assumes that we have abstract “units” whose states are symmetrically exchangeable. But neuroscientists know that these units are *neurons*, whose individual and collective properties are *asymmetric* with respect to state exchanges, for biophysical reasons. The prior of the inhibited model  $P_i$  reflects this asymmetry. It is fortunate that we can partially correct the symmetry assumption of bare maximum-entropy by using a prior, without having to overturn our whole space of variables.

The long argument above shows, we hope, that the inhibited model  $P_i$  and its reference prior do not break the “non-committal” nature of the maximum-entropy principle; rather, they prevent maximum-entropy from committing to unrealistic assumptions. The inhibited model can therefore be quite useful as a realistic hypothesis against which to check or measure the prominence of correlations in simulated or recorded neural activities.

### 3.3 Back to the big picture

Let us conclude by returning to the general modelling point of view outlined in the Introduction. Our original goal was to simplify  $P(\text{activity}|\text{stimuli})$  via a set of intermediate models  $\{M\}$ , each with a multi-dimensional parameter  $\alpha$ , by  $P(\text{activity}|\text{state}) = \sum_M \int P(\text{activity}|\alpha, M) P(\alpha, M|\text{state}) d\alpha$ . They should be neurobiologically sound but mathematically manageable. The next step is to establish which of these models is most probable, given the observed activities:

$$P(\alpha, M|\text{activity}) \propto P(\text{activity}|\alpha, M) P(\alpha, M), \quad (36)$$

where  $P(\alpha, M)$  are the prior probabilities we assign to these models. The determining factor is usually  $P(\text{activity}|\alpha, M)$ , called the *evidence*. This last step is adamantly explained and discussed in a beautiful paper by Mackay [158]. The pairwise maximum-entropy model  $P_p$ , and the inhibited pairwise maximum-entropy model  $P_i$  presented in this paper, are two examples of such “ $M$ ”. And we can consider higher-moment maximum-entropy models, models with deeper underlying assumptions, and even models not based on maximum-entropy at all. It is against this last step that the question of the importance of pairwise and higher-order correlations, and of maximum-entropy models in general, acquires its full meaning and can be given a precise answer.

## 4 Materials and Methods

### 4.1 Definition of Glauber dynamics

We now show that there is a temporal process that is able to sample from the the distribution  $P_p(\mathbf{s}|\boldsymbol{\mu}, \boldsymbol{\Lambda})$  eq. (6). This temporal dynamics is called *Glauber dynamics*. It is an example of a Markov chain on the space of binary spins  $\{0, 1\}^N$  [69]. At each time step a spin  $s_i$  is chosen randomly and updated with the update rule

$$s_i \leftarrow 1 \text{ with probability } F_i(s) = g\left(\sum_j \Lambda_{ij}s_j + \mu_i\right) \text{ and } 0 \text{ else} \quad (37)$$

$$g(x) = \frac{1}{1 + \exp(-x)}, \quad (38)$$

where the coupling is assumed to be symmetric,  $\Lambda_{ij} = \Lambda_{ji}$ , and self-coupling is absent,  $\Lambda_{ii} = 0$ . The transition operator of the Markov chain,  $\kappa$ , only connects states that differ by at most one spin, so for the transition of spin  $i$  we can write, if  $s^{i+} = (s_1, \dots, \underbrace{1}_{i\text{-th}}, \dots, s_N)$  and  $s^{i-} = (s_1, \dots, \underbrace{0}_{i\text{-th}}, \dots, s_N)$ ,

$$\begin{aligned} \kappa(s^{i+}|s^{i-}) &= F_i(s^{i-}) \\ \kappa(s^{i-}|s^{i+}) &= 1 - F_i(s^{i+}). \end{aligned} \quad (39)$$

The pairwise maximum-entropy distribution  $P_p(\mathbf{s}|\boldsymbol{\mu}, \boldsymbol{\Lambda})$  is stationary under the Markov dynamics above. The proof can be obtained as the  $\Lambda_I = 0$  case of the proof, given below, for the inhibited pairwise maximum-entropy model.

### 4.2 Inhibited Glauber dynamics and its stationary maximum-entropy distribution

#### 4.2.1 Inhibited Glauber dynamics.

In the ‘‘inhibited’’ Glauber dynamics, the network of  $N$  neurons with states  $s_i(t)$  has an additional neuron with state  $s_I(t)$ . The dynamics is determined by the following algorithm starting at time step  $t$  with states  $\mathbf{s} = \mathbf{s}(t)$ ,  $s_I = s_I(t)$ :

Step 1. One of the  $N$  units is chosen, each unit having probability  $1/N$  of being the chosen one. Suppose  $i$  is the selected unit.

Step 2. The chosen unit  $i$  is updated to the state  $s'_i := s_i(t+1)$  with probability

$$\begin{aligned} p(s'_i | \mathbf{s}, s_I) &= (1 + \exp[(1 - 2s'_i)F_i(\mathbf{s}, s_I)])^{-1} \\ &= \begin{cases} [1 + e^{F_i(\mathbf{s}, s_I)}]^{-1}, & \text{for } s'_i = 0, \\ [1 + e^{-F_i(\mathbf{s}, s_I)}]^{-1}, & \text{for } s'_i = 1, \end{cases} \\ \text{with } F_i(\mathbf{s}, s_I) &:= \mu_i + \sum_{k \neq i}^{k \neq i} \Lambda_{ik} s_k / 2 + \Lambda_I s_I. \end{aligned}$$

Note the additional coupling from the neuron  $s_I$ , with strength  $\Lambda_I$ . This strength can have any sign, but we are interested in the  $\Lambda_I \leq 0$  case; we therefore call  $s_I$  the “inhibitory neuron”.

Step 3. The inhibitory neuron is deterministically updated to the state  $s'_I := s_I(t+1)$  given by

$$s'_I = H\left(\sum_k s_k / N - \theta\right), \quad (40)$$

corresponding to a Kronecker-delta conditional probability

$$p(s'_I | \mathbf{s}, s_I) = p(s'_I | \mathbf{s}) = \delta[s'_I - H(\sum_k s_k / N - \theta)]. \quad (41)$$

In other words, the inhibitory neuron becomes active if the population-averaged activity of the other neurons is equal to or exceeds the threshold  $\theta$ .

Step 4. The time is stepped forward,  $t+1 \rightarrow t$ , and the process repeats from step 1.

The original Glauber dynamics, described in the previous section, is recovered when  $\Lambda_I = 0$ , which corresponds to decoupling the inhibitory neuron  $s_I$ .

The total transition probability can be written as

$$\begin{aligned} p(\mathbf{s}', \mathbf{s}'_I | \mathbf{s}, s_I) &= \frac{1}{N} \delta[s'_I - H(\sum_k s_k / N - \theta)] \times \\ &\quad \sum_i \left[ (1 + \exp[(1 - 2s'_i)F_i(\mathbf{s}, s_I)])^{-1} \prod_{k \neq i}^{k \neq i} \delta(s'_k - s_k) \right]; \quad (42) \end{aligned}$$

the product of Kronecker deltas in the last term ensures that at most one of the  $N$  neurons changes state at each timestep.

The transition probabilities for the chosen neuron  $s_i$  and the inhibitory neuron  $s_I$  are independent, conditional on the state of the network at the previous timestep:

$$p(\mathbf{s}', s'_I | \mathbf{s}, s_I) = p(\mathbf{s}' | \mathbf{s}) p(s'_I | \mathbf{s}),$$

so the transition probability for the  $N$  neurons only can be written as

$$p(\mathbf{s}' | \mathbf{s}) = \frac{1}{N} \sum_i \left[ (1 + \exp[(1 - 2s'_i)F_i(\mathbf{s})])^{-1} \prod_{k \neq i}^{k \neq i} \delta(s'_k - s_k) \right], \quad (43)$$

$$\text{with } F_i(\mathbf{s}) := \mu_i + \sum_{k \neq i}^{k \neq i} \Lambda_{ik} s_k / 2 + \Lambda_I H(\sum_k s_k / N - \theta). \quad (44)$$

#### 4.2.2 Proof that the inhibited maximum-entropy model is the stationary distribution of the inhibited Glauber dynamics.

The modified maximum-entropy distribution  $P_i$ , eq. (26), is the stationary distribution of a slightly modified version of the above dynamics, with the update rule

$$s'_I = H\left(\sum_k^{k \neq i} s_k / N - \theta\right), \quad (45)$$

and the use of  $N$  inhibitory neurons, one for each of the original  $N$  units. This dynamics has a slightly different transition probability, with activation function

$$F_i(\mathbf{s}) := \mu_i + \sum_k^{k \neq i} \Lambda_{ik} s_k / 2 + \Lambda_I H(\sum_k^{k \neq i} s_k / N - \theta) \quad (46)$$

instead of eq. (44). Note that the two dynamics are very similar for large enough  $N$ . To prove the stationarity of inhibited maximum-entropy distribution  $P_i$ , we show that  $P_i$  satisfies the detailed-balance equality

$$p(\mathbf{s}' | \mathbf{s}) P_i(\mathbf{s}) = p(\mathbf{s} | \mathbf{s}') P_i(\mathbf{s}') \quad \text{or} \quad \frac{p(\mathbf{s}' | \mathbf{s})}{p(\mathbf{s} | \mathbf{s}')} = \frac{P_i(\mathbf{s}')}{P_i(\mathbf{s})}, \quad \forall \mathbf{s}, \mathbf{s}', \quad (47)$$

which is a sufficient condition for stationarity [196–198].

First note that if  $\mathbf{s}'$  and  $\mathbf{s}$  differ in the state of more than one neuron, the transition probability  $p(\mathbf{s}' | \mathbf{s})$  vanishes and the detailed-balance above is

trivially satisfied. Also the case  $\mathbf{s}' = \mathbf{s}$  is trivially satisfied. Only the case in which  $\mathbf{s}'$  and  $\mathbf{s}$  differ in the state of one unit, say  $s_i$ , remains to be proven. Assume then that

$$s'_i = 1, \quad s_i = 0, \quad \forall k \neq i, \quad s'_k = s_k; \quad (48)$$

by symmetry, if the detailed balance is satisfied in the case above it will also be satisfied with the values 0 and 1 interchanged.

Substituting the transition probability eq. (43) and eq. (46) in the left-hand side of the fraction form of the detailed balance eq. (47), and noting that  $F_i(\mathbf{s}') = F_i(\mathbf{s})$ , we have

$$\begin{aligned} \frac{p(\mathbf{s}' | \mathbf{s})}{p(\mathbf{s} | \mathbf{s}')} &= \exp[-F_i(\mathbf{s})]^{-1} \\ &= \exp \left[ \mu_i + \sum_k^{k \neq i} \Lambda_{ik} s_k / 2 + \Lambda_I \text{H} \left( \sum_k^{k \neq i} s_k / N - \theta \right) \right]. \end{aligned} \quad (49)$$

Using the expression for the inhibited model  $P_1$ , eq. (26), in the right-hand side of the fraction form of the detailed balance eq. (47), we have

$$\begin{aligned} \frac{P(\mathbf{s}')}{P(\mathbf{s})} &= \exp \left[ \mu_i + \sum_k^{k \neq i} \mu_k s_k + \frac{1}{2} \sum_k^{k \neq i} \Lambda_{ik} s_k + \right. \\ &\quad \left. \frac{1}{2} \sum_{k, m \neq i}^{k < m} \Lambda_{mk} s_m s_k + \Lambda_I N G \left( \sum_k^{k \neq i} \frac{s_k}{N} + \frac{1}{N} - \theta \right) \right] \\ &= \exp \left[ \mu_i + \frac{1}{2} \sum_k^{k \neq i} \Lambda_{ik} s_k + \Lambda_I \text{H} \left( \sum_k^{k \neq i} s_k / N - \theta \right) \right], \end{aligned} \quad (50)$$

where we have used the equality  $NG(x + 1/N) - NG(x) = \text{H}(x)$ , valid if  $x = \sum_k^{k \neq i} s_k / N - \theta$  and  $N\theta \in \mathbf{Z}$ . Comparison of formulae eq. (49) and eq. (50) finally proves that the detailed balance is satisfied also in the case eq. (48).

### 4.3 Simulation of Glauber dynamics with NEST

The neuron model `ginzburg_neuron` in NEST implements the Glauber dynamics, if the parameters of the gain function are chosen appropriately.

The gain function has the form

$$g_{\text{ginzburg}}(h) = c_1 h + \frac{c_2}{2}(1 + \tanh(c_3(h - \theta))). \quad (51)$$

With  $\tanh(x) = \frac{e^x - e^{-x}}{e^x + e^{-x}}$ , setting  $x = c_3(h - \theta)$ ,  $c_1 = 0$ ,  $c_2 = 1$ ,  $c_3 = \frac{1}{2}$  it takes the form

$$\begin{aligned} g_{\text{ginzburg}}(h) &= \frac{1}{2} \frac{e^x + e^{-x} + e^x - e^{-x}}{e^x + e^{-x}}, \\ &= \frac{1}{1 + e^{-2x}} = \frac{1}{1 + e^{-(h-\theta)}}, \end{aligned} \quad (52)$$

which is identical to eq. (38).

## Acknowledgements

We are grateful to Alexa Riehle and Thomas Brochier for providing the experimental data and to Sonja Grün for fruitful discussions on their interpretation. The work was carried out in the framework of the joint International Associated Laboratory (LIA) of INT (CNRS, AMU), Marseilles and INM-6, Jülich. Partially supported by HGF young investigator's group VH-NG- 1028, Helmholtz portfolio theme SMHB, and EU Grant 604102 (Human Brain Project, HBP). All network simulations carried out with NEST (<http://www.nest-simulator.org>).

PGLPM thanks the Forschungszentrum librarians for their always prompt and efficient help in finding arcane scientific works, Miri & Mari for encouragement and affection, Buster for filling life with awe and inspiration, and the developers and maintainers of L<sup>A</sup>T<sub>E</sub>X, Emacs, AUC<sub>T</sub>E<sub>X</sub>, MiK<sub>T</sub>E<sub>X</sub>, Lyx, Inkscape, bioRxiv, arXiv, HAL, PhilSci, Sci-Hub for making a free and unfiltered science possible.

## Bibliography

1. A Arieli, A Sterkin, A Grinvald, and A Aertsen. Dynamics of ongoing activity: explanation of the large variability in evoked cortical responses. *Science*, 273(5283): 1868–1871, Sep 1996.
2. Eric R. Kandel, James H. Schwartz, Thomas M. Jessell, Steven A. Siegelbaum, and A. J. Hudspeth, editors. *Principles of Neural Science*. McGraw-Hill, New York, 5 edition, 2013.

3. Peter E. Latham and Yasser Roudi. Role of correlations in population coding. In [13], chapter 7, pages 121–138. 2013. [arXiv:1109.6524](https://arxiv.org/abs/1109.6524).
4. A. Philip Dawid. Conditional independence in statistical theory. *J. Roy. Stat. Soc. B*, 41(1):1–31, 1979. With discussion by D. V. Lindley, A. D. McLaren, J. B. Kadane, J. M. Dickey, S. M. Rizvi, E. F. Harding, G. A. Barnard, P. J. Bickel, M. H. DeGroot, D. A. S. Fraser, R. F. Galbraith, S. Geisser, V. P. Godambe, D. V. Hinkley, H. Kudō, K. V. Mardia, M. Mouchart, I. Nimmo-Smith, M. R. Novick, Donald B. Rubin, R. A. Wijsman, and the author; <http://distancecovariance.googlecode.com/svn/trunk/References/Conditional%20Independence%20in%20Statistical%20Theory.pdf>.
5. Wolfgang Spohn. Stochastic independence, causal independence, and shieldability. *J. Philos. Logic*, 9(1):73–99, 1980. [http://www.uni-konstanz.de/philosophie/files/06\\_spohn\\_stochastic\\_\\_1c403d.pdf](http://www.uni-konstanz.de/philosophie/files/06_spohn_stochastic__1c403d.pdf).
6. Judea Pearl. *Probabilistic Reasoning in Intelligent Systems: Networks of Plausible Inference*. The Morgan Kaufmann series in representation and reasoning. Morgan Kaufmann, San Francisco, rev. second printing edition, 1988.
7. Judea Pearl. *Causality: Models, Reasoning, and Inference*. Cambridge University Press, Cambridge, 2000. Parts available at <http://bayes.cs.ucla.edu/BOOK-2K/>.
8. Carlton M. Caves. Learning and the de Finetti representation, 2000. <http://info.phys.unm.edu/~caves/reports/reports.html>.
9. David Ferster and Nelson Spruston. Cracking the neuronal code. *Science*, 270(5237):756–757, 1995.
10. Alexander Borst and Frédéric E. Theunissen. Information theory and neural coding. *Nat. Neurosci.*, 2(11):947–957, 1999.
11. Stefano Panzeri, Simon R. Schultz, Alessandro Treves, and Edmund T. Rolls. Correlations and the encoding of information in the nervous system. *Proc. R. Soc. Lond. B*, 266(1423):1001–1012, 1999. <http://people.sissa.it/~ale/Pan+99a.pdf>.
12. Kenji Doya, Shin Ishii, Alexandre Pouget, and Rajesh P. N. Rao. *Bayesian Brain: Probabilistic Approaches to Neural Coding*. Computational neuroscience. The MIT Press, Cambridge, USA, 2007.
13. Rodrigo Quian Quiroga and Stefano Panzeri, editors. *Principles of Neural Coding*. CRC Press, Boca Raton, USA, 2013.
14. Stefano Panzeri, Jakob H. Macke, Joachim Gross, and Christoph Kayser. Neural population coding: combining insights from microscopic and mass signals. *Trends Cognit. Sci.*, 19(3):162–172, 2015.

15. David A. Freedman. Invariants under mixing which generalize de Finetti's theorem. *Ann. Math. Stat.*, 33(3):916–923, 1962.
16. A. Philip Dawid. Intersubjective statistical models. In [199], pages 287–232. 1982.
17. Steffen L. Lauritzen. Extreme point models in statistics. *Scand. J. Statist.*, 11(2): 65–91, 1984. With discussion by Ole E. Barndorff-Nielsen, A. Philip Dawid and Persi Diaconis, Søren Johansen, and reply.
18. Steffen L. Lauritzen. *Extremal Families and Systems of Sufficient Statistics*, volume 49 of *Lecture notes in statistics*. Springer, Berlin, 1988.
19. G. Larry Bretthorst. The maximum entropy method of moments and Bayesian probability theory. *Am. Inst. Phys. Conf. Proc.*, 1553:3–15, 2013. <http://bayes.wustl.edu/glb/BretthorstHistograms.pdf>.
20. A. Philip Dawid. Exchangeability and its ramifications. In [200], chapter 2, pages 19–29. 2013.
21. Claude Elwood Shannon. A mathematical theory of communication. *Bell Syst. Tech. J.*, 27(3, 4):379–423, 623–656, 1948. <http://cm.bell-labs.com/cm/ms/what/shannonday/paper.html>, <http://www.cparity.com/it/demo/external/shannon.pdf>.
22. Claude Elwood Shannon. Communication in the presence of noise. *Proc. IRE*, 37(1):10–21, 1949. Repr. in [201].
23. Edwin Thompson Jaynes. Information theory and statistical mechanics. *Phys. Rev.*, 106(4):620–630, 1957. <http://bayes.wustl.edu/etj/node1.html>, see also [202].
24. Edwin Thompson Jaynes. Information theory and statistical mechanics. In [203], pages 181–218. 1963. Repr. in [204, chap. 4, pp. 39–76]; <http://bayes.wustl.edu/etj/node1.html>.
25. Edwin Thompson Jaynes. Foundations of probability theory and statistical mechanics. In [205], pages 77–101. 1967. <http://bayes.wustl.edu/etj/node1.html>.
26. Arthur Hobson. A new theorem of information theory. *J. Stat. Phys.*, 1(3):383–391, 1969.
27. Myron Tribus. *Rational Descriptions, Decisions and Designs*. Pergamon, New York, 1969.
28. Arthur Hobson and Bin-Kang Cheng. A comparison of the Shannon and Kullback information measures. *J. Stat. Phys.*, 7(4):301–310, 1973.

29. Stephen F. Gull and G. J. Daniell. Image reconstruction from incomplete and noisy data. *Nature*, 272(5655):686–690, 1978.
30. Edwin Thompson Jaynes. On the rationale of maximum-entropy methods. *Proc. IEEE*, 70(9):939, 1982. <http://bayes.wustl.edu/etj/node1.html>.
31. Imre Csiszár. Sanov property, generalized  $I$ -projection and a conditional limit theorem. *Ann. Prob.*, 12(3):768–793, 1984.
32. Lawrence R. Mead and N. Papanicolaou. Maximum entropy in the problem of moments. *J. Math. Phys.*, 25(8):2404–2417, 1984. <http://bayes.wustl.edu/Manual/MeadPapanicolaou.pdf>.
33. Edwin Thompson Jaynes. Where do we go from here? In [206], pages 21–58. 1985. <http://bayes.wustl.edu/etj/node1.html>.
34. Imre Csiszár. An extended maximum entropy principle and a Bayesian justification. In [207], pages 83–98, 1985.
35. Edwin Thompson Jaynes. Monkeys, kangaroos, and  $N$ , 1996. <http://bayes.wustl.edu/etj/node1.html>; first publ. 1986. (Errata: in equations (29)–(31), (33), (40), (44), (49) the commas should be replaced by gamma functions, and on p. 19 the value 0.915 should be replaced by 0.0915).
36. Devinderjit Singh Sivia. Bayesian inductive inference, maximum entropy, & neutron scattering. *Los Alamos Science*, 4(19):180–207, 1990. <http://www.fas.org/sgp/othersgov/doe/lanl/pubs/number19.htm>.
37. John Skilling. Quantified maximum entropy. In [208], pages 341–350, 1990.
38. Edwin Thompson Jaynes. *Probability Theory: The Logic of Science*. Cambridge University Press, Cambridge, 2003. Ed. by G. Larry Bretthorst; <http://omega.albany.edu:8008/JaynesBook.html>, <http://omega.albany.edu:8008/JaynesBookPdf.html>, <http://www-biba.inrialpes.fr/Jaynes/prob.html>; first publ. 1994.
39. Hans-Otto Georgii. Probabilistic aspects of entropy. In [209], chapter 3, pages 37–54. 2003. <http://www.mathematik.uni-muenchen.de/~georgii/papers/Dresden.pdf>.
40. Imre Csiszár and Paul C. Shields. Information theory and statistics: A tutorial. *Foundations and Trends in Communications and Information Theory*, 1(4):417–528, 2004. <http://www.renyi.hu/~csiszar/>.
41. S. M. Bohte, H. Spekreijse, and P. R. Roelfsema. The effects of pair-wise and higher-order correlations on the firing rate of a postsynaptic neuron. *Neural Comp.*, 12(1):153–179, 2000.

42. Elad Schneidman, Michael J. Berry II, Ronen Segev, and William Bialek. Weak pairwise correlations imply strongly correlated network states in a neural population. *Nature*, 440(7087):1007–1012, 2006. [arXiv:q-bio/0512013](https://arxiv.org/abs/q-bio/0512013), [http://www.weizmann.ac.il/neurobiology/labs/schneidman/The\\_Schneidman\\_Lab/Publications.html](http://www.weizmann.ac.il/neurobiology/labs/schneidman/The_Schneidman_Lab/Publications.html).
43. Gašper Tkačik, Elad Schneidman, Michael J. Berry II, and William Bialek. Ising models for networks of real neurons, 2006. [arXiv:q-bio/0611072](https://arxiv.org/abs/q-bio/0611072).
44. Marlene R. Cohen and Adam Kohn. Measuring and interpreting neuronal correlations. *Nat. Neurosci.*, 14(7):811–819, 2011. <http://marlenecohen.com/pubs/CohenKohn2011.pdf>.
45. Einat Granot-Atedgi, Gašper Tkačik, Ronen Segev, and Elad Schneidman. Stimulus-dependent maximum entropy models of neural population codes. *PLoS Computational Biology*, 9(3):e1002922, 2013. [arXiv:1205.6438](https://arxiv.org/abs/1205.6438).
46. L. Martignon, H. Von Hasse, Sonja Grün, Ad Aertsen, and Günther Palm. Detecting higher-order interactions among the spiking events in a group of neurons. *Biol. Cybern.*, 73(1):69–81, 1995.
47. Jonathon Shlens, Greg D. Field, Jeffrey L. Gauthier, Matthew I. Grivich, Dumitru Petrusca, Alexander Sher, Alan M. Litke, and E. J. Chichilnisky. The structure of multi-neuron firing patterns in primate retina. *J. Neurosci.*, 26(32):8254–8266, 2006. See also correction [210].
48. Jakob H. Macke, Manfred Oppen, and Matthias Bethge. The effect of pairwise neural correlations on global population statistics. Technical Report 183, Max-Planck-Institut für biologische Kybernetik, Tübingen, 2009. [http://www.kyb.tuebingen.mpg.de/publications/attachments/MPIK-TR-183\\_%5B0%5D.pdf](http://www.kyb.tuebingen.mpg.de/publications/attachments/MPIK-TR-183_%5B0%5D.pdf).
49. Andrea K. Barreiro, Julijana Gjorgjieva, Fred Rieke, and Eric Shea-Brown. When do microcircuits produce beyond-pairwise correlations?, 2010. [arXiv:1011.2797](https://arxiv.org/abs/1011.2797).
50. Elad Ganmor, Ronen Segev, and Elad Schneidman. Sparse low-order interaction network underlies a highly correlated and learnable neural population code. *Proc. Natl. Acad. Sci. (USA)*, 108(23):9679–9684, 2011. [http://www.weizmann.ac.il/neurobiology/labs/schneidman/The\\_Schneidman\\_Lab/Publications.html](http://www.weizmann.ac.il/neurobiology/labs/schneidman/The_Schneidman_Lab/Publications.html).
51. Hideaki Shimazaki, Kolia Sadeghi, Tomoe Ishikawa, Yuji Ikegaya, and Taro Toyozumi. Simultaneous silence organizes structured higher-order interactions in neural populations. *Sci. Rep.*, 5:9821, 2015.
52. Yasser Roudi, Joanna Tyrcha, and John Hertz. Ising model for neural data: Model quality and approximate methods for extracting functional connectivity. *Phys. Rev. E*, 79(5):051915, 2009. [arXiv:0902.2885](https://arxiv.org/abs/0902.2885).

53. Sebastian Gerwinn, Jakob H. Macke, and Matthias Bethge. Bayesian inference for generalized linear models for spiking neurons. *Front. Comput. Neurosci.*, 4:12, 2010.
54. Jakob H. Macke, Lars Buesing, John P. Cunningham, Byron M. Yu, Krishna V. Shenoy, and Maneesh Sahani. Empirical models of spiking in neural populations. *Advances in Neural Information Processing Systems (NIPS proceedings)*, 24:1350–1358, 2011.
55. Jakob H. Macke, Iain Murray, and Peter E. Latham. Estimation bias in maximum entropy models. *Entropy*, 15(8):3109–3129, 2013. <http://www.gatsby.ucl.ac.uk/~pel/papers/maxentbias.pdf>.
56. C. Alden Mead. The special role of maximum entropy in the application of “mixing character” to irreversible processes in macroscopic systems. In [211], pages 273–287. 1979.
57. Shu-Cherng Fang, J. R. Rajasekera, and H.-S. J. Tsao. *Entropy optimization and mathematical programming*, volume 8 of *International series in operations research & management science*. Springer, New York, reprint edition, 1997.
58. R. Tyrrell Rockafellar. Lagrange multipliers and optimality. *SIAM Rev.*, 35(2):183–238, 1993. <http://www.math.washington.edu/~rtr/papers.html>.
59. William H. Press, Saul A. Teukolsky, William T. Vetterling, and Brian P. Flannery. *Numerical Recipes: The Art of Scientific Computing*. Cambridge University Press, Cambridge, 3 edition, 2007. First publ. 1988.
60. M. A. L. Nicolelis, editor. *Methods for Neural Ensemble Recordings*. CRC Press, Boca Raton, Florida, 1998.
61. György Buzsáki. Large-scale recording of neuronal ensembles. *Nat. Neurosci.*, 7(5):446–451, May 2004.
62. Antal Berényi, Zoltán Somogyvári, Anett J. Nagy, Lisa Roux, John D. Long, Shigeyoshi Fujisawa, Eran Stark, Anthony Leonardo, Timothy D. Harris, and György Buzsáki. Large-scale, high-density (up to 512 channels) recording of local circuits in behaving animals. *J. Neurophysiol.*, 111(5):1132–1149, 2014. <http://www.buzsakilab.com/content/PDFs/Berenyi2013.pdf>.
63. F. James. Monte Carlo theory and practice. *Rep. Prog. Phys.*, 43(9):1145–1189, 1980.
64. Kurt Binder, editor. *Applications of the Monte Carlo Method in Statistical Physics*, volume 36 of *Topics in current physics*. Springer, Berlin, 2 edition, 1987. First publ. 1984.

65. David J. C. MacKay. *Information Theory, Inference, and Learning Algorithms*. Cambridge University Press, Cambridge, 2003. <http://www.inference.phy.cam.ac.uk/mackay/itila/>; first publ. 1995.
66. David P. Landau and Kurt Binder. *A Guide to Monte Carlo Simulations in Statistical Physics*. Cambridge University Press, Cambridge, 4 edition, 2015. [http://el.us.edu.pl/ekonofizyka/images/6/6b/A\\_guide\\_to\\_monte\\_carlo\\_simulations\\_in\\_statistical\\_physics.pdf](http://el.us.edu.pl/ekonofizyka/images/6/6b/A_guide_to_monte_carlo_simulations_in_statistical_physics.pdf), [http://iop.vast.ac.vn/~nvthanh/cours/simulation/MC\\_book.pdf](http://iop.vast.ac.vn/~nvthanh/cours/simulation/MC_book.pdf). First publ. 2000.
67. Christophe Andrieu, Nando de Freitas, Arnaud Doucet, and Michael I. Jordan. An introduction to MCMC for machine learning. *Mach. Learn.*, 50(1–2):5–43, 2003. <http://cis.temple.edu/~latecki/Courses/RobotFall07/PapersFall07/andrieu03introduction.pdf>.
68. Werner Krauth. *Statistical Mechanics: Algorithms and Computations*. Oxford master series in statistical, computational, and theoretical physics. Oxford University Press, Oxford, 2006.
69. Roy J. Glauber. Time-dependent statistics of the Ising model. *J. Math. Phys.*, 4(2):294–307, 1963.
70. David H. Ackley, Geoffrey E. Hinton, and Terrence J. Sejnowski. A learning algorithm for Boltzmann machines. *Cognit. Sci.*, 9(1):147–169, 1985.
71. G. E. Hinton and T. J. Sejnowski. Learning and relearning in Boltzmann machines. In [212], chapter 7, pages 282–317, 507–516. 1999. First publ. 1986; <https://papers.cnl.salk.edu/PDFs/Learning%20and%20Relearning%20in%20Boltzmann%20Machines%201986-3239.pdf>.
72. Tamara Broderick, Miroslav Dudik, Gašper Tkačik, Robert E. Schapire, and William Bialek. Faster solutions of the inverse pairwise Ising problem, 2007. [arXiv:0712.2437](https://arxiv.org/abs/0712.2437).
73. Douglas Rayne Hartree. The wave mechanics of an atom with a non-coulomb central field. Part I. Theory and methods. *Proc. Cambridge Philos. Soc.*, 24(1): 89–110, 1928. <http://sci-prew.inf.ua/index1.htm>; see also [213].
74. John W. Negele and Henri Orland. *Quantum Many-Particle Systems*. Advanced book classics. Perseus Books, Reading, USA, 1998. First publ. 1988.
75. Manfred Opper and David Saad, editors. *Advanced Mean Field Methods: Theory and Practice*. Neural information processing series. The MIT Press, Cambridge, USA, 2001.
76. D. J. Thouless, P. W. Anderson, and R. G. Palmer. Solution of ‘Solvable model of a spin glass’. *Phil. Mag.*, 35(3):593–601, 1977.

77. Vitor Sessak and Rémi Monasson. Small-correlation expansions for the inverse Ising problem. *J. Phys. A*, 42(5):055001, 2009. [arXiv:0811.3574](#).
78. Vitor Sessak. *Inverse problems in spin models*. PhD thesis, École Normale Supérieure, Paris, 2010. [arXiv:1010.1960](#).
79. Sonja Grün. Data-driven significance estimation for precise spike correlation. *J. Neurophysiol.*, 101(3):1126–1140, 2009.
80. Jakob H. Macke, Philipp Berens, Alexander S. Ecker, Andreas S. Tolias, and Matthias Bethge. Generating spike trains with specified correlation coefficients. *Neural Comp.*, 21(2):397–423, 2009.
81. Shigeyoshi Fujisawa, Asohan Amarasingham, Matthew T. Harrison, and György Buzsáki. Behavior-dependent short-term assembly dynamics in the medial prefrontal cortex. *Nat. Neurosci.*, 11(7):823–833, 2008.
82. S. Grün, A. Riehle, and M. Diesmann. Effect of cross-trial nonstationarity on joint-spike events. *Biol. Cybern.*, 88(5):335–351, 2003.
83. G. Pipa and S. Grün. Non-parametric significance estimation of joint-spike events by shuffling and resampling. *Neurocomputing*, 52–54:31–37, 2003.
84. Gordon Pipa, Markus Diesmann, and Sonja Grün. Significance of joint-spike events based on trial-shuffling by efficient combinatorial methods. *Complexity*, 8(4):79–86, 2003.
85. G. L. Gerstein. Searching for significance in spatio-temporal firing patterns. *Acta Neurobiol. Exp.*, 64:203–207, 2004.
86. Yasser Roudi, Sheila Nirenberg, and Peter E. Latham. Pairwise maximum entropy models for studying large biological systems: When they can work and when they can’t. *PLoS Computational Biology*, 5(5):e1000380, 2009. [arXiv:0811.0903](#).
87. Gašper Tkačik, Elad Schneidman, Michael J. Berry II, and William Bialek. Spin glass models for a network of real neurons, 2009. [arXiv:0912.5409](#).
88. Gašper Tkačik, Thierry Mora, Olivier Marre, Dario Amodei, Stephanie E. Palmer, Michael J. Berry II, and William Bialek. Thermodynamics and signatures of criticality in a network of neurons. *Proc. Natl. Acad. Sci. (USA)*, 112(37):11508–11513, 2014. [arXiv:1407.5946](#).
89. Thierry Mora, Stéphane Deny, and Olivier Marre. Dynamical criticality in the collective activity of a population of retinal neurons. *Phys. Rev. Lett.*, 114(7):078105, 2015. [arXiv:1410.6769](#).

90. Jakob H. Macke, Manfred Oppen, and Matthias Bethge. Common input explains higher-order correlations and entropy in a simple model of neural population activity. *Phys. Rev. Lett.*, 106(20):208102, 2011. [arXiv:1009.2855](#).
91. Solomon Kullback. *Information Theory and Statistics*. Dover, New York, 1978. Republ. with a new preface and corrections and additions by the author; first publ. 1959.
92. Solomon Kullback and John C. Keegel. Categorical data problems using information theoretic approach. In [214], chapter 35, pages 831–873. 1984.
93. L. L. Campbell. The relation between information theory and the differential geometry approach to statistics. *Inf. Sci.*, 35(3):199–210, 1985.
94. Solomon Kullback and R. A. Leibler. On information and sufficiency. *Ann. Math. Stat.*, 22(1):79–86, 1951.
95. Alfred Rényi. On measures of entropy and information. In [215], pages 547–561. 1961.
96. Nikolaï Nikolaevič Čencov [Chentsov]. *Statistical Decision Rules and Optimal Inference*, volume 53 of *Translations of mathematical monographs*. American Mathematical Society, Providence, USA, 1982. Transl. by Lev J. Leifman; first publ. in Russian 1972.
97. Janos Aczél and Z. Daróczy. *On Measures of Information and Their Characterizations*, volume 115 of *Mathematics in science and engineering*. Academic Press, New York, 1975.
98. Stephen F. Gull and John Skilling. The maximum entropy method. In [216], pages 267–279. 1984.
99. Stephen F. Gull and John Skilling. Maximum entropy method in image processing. *IEE Proc. F*, 131(6):646–659, 1984.
100. Solomon Kullback, John C. Keegel, and Joseph H. Kullback. *Topics in Statistical Information Theory*, volume 42 of *Lecture notes in statistics*. Springer, Berlin, 1987.
101. Solomon Kullback. The Kullback-Leibler distance. *American Statistician*, 41(4):340–341, 1987.
102. Stephen F. Gull and John Skilling. Quantified maximum entropy: MemSys5. Users’ manual. Technical report, Maximum Entropy Data Consultants, Suffolk, UK, 1999. <http://www.mpe.mpg.de/~aws/integral/issw/memsys5.pdf>; first publ. 1990.
103. John C. Baez and Tobias Fritz. A Bayesian characterization of relative entropy. *Theory and Applications of Categories*, 29(16):421–456, 2014. [arXiv:1402.3067](#).

104. ISO. *ISO 80000:2009: Quantities and units*. International Organization for Standardization, Geneva, 2009.
105. Joint Committee for Guides in Metrology (JCGM). *JCGM 100:2008: Evaluation of measurement data – Guide to the expression of uncertainty in measurement*. BIPM, IEC, IFCC, ILAC, ISO, IUPAC, IUPAP, OIML, corr. version edition, 2010. <http://www.bipm.org/en/publications/guides/gum.html>. First publ. 1993. See also [106, 107, 217–219].
106. Joint Committee for Guides in Metrology (JCGM). *JCGM 101:2008: Evaluation of measurement data – Supplement 1 to the “Guide to the expression of uncertainty in measurement” – Propagation of distributions using a Monte Carlo method*. BIPM, IEC, IFCC, ILAC, ISO, IUPAC, IUPAP, OIML, 2008. <http://www.bipm.org/en/publications/guides/gum.html>. See [105].
107. Joint Committee for Guides in Metrology (JCGM). *JCGM 200:2012: International vocabulary of metrology – Basic and general concepts and associated terms (VIM)*. BIPM, IEC, IFCC, ILAC, ISO, IUPAC, IUPAP, OIML, 3 edition, 2012. <http://www.bipm.org/en/publications/guides/vim.html>. First publ. 1993. See also [105].
108. ISO. *ISO 3534-1:2006: Statistics – Vocabulary and symbols – Part 1: General statistical terms and terms used in probability*. International Organization for Standardization, Geneva, 2006.
109. ISO. *ISO 3534-2:2006: Statistics – Vocabulary and symbols – Part 2: Applied statistics*. International Organization for Standardization, Geneva, 2006.
110. NIST. *Guidelines for Evaluating and Expressing the Uncertainty of NIST Measurement Results: NIST technical note 1297, 1994 edition*. National Institute of Standards and Technology, Washington, D.C., 1994. <http://physics.nist.gov/cuu/Uncertainty/bibliography.html>.
111. NIST. *Guide for the Use of the International System of Units (SI): NIST special publication 811, 1995 edition*. National Institute of Standards and Technology, Washington, D.C., 1995. <http://physics.nist.gov/cuu/Uncertainty/bibliography.html>.
112. Elad Schneidman, Michael J. Berry, Ronen Segev, and William Bialek. Weak pairwise correlations imply strongly correlated network states in a neural population. *Nature*, 440:1007–1012, April 2006.
113. Jonathon Shlens, Greg D Field, Jeffrey L Gauthier, Matthew I Grivich, Dumitru Petrusca, Alexander Sher, Alan M Litke, and EJ Chichilnisky. The structure of multi-neuron firing patterns in primate retina. *Journal of Neuroscience*, 26(32): 8254–8266, 2006.

114. Anthony J. M. Garrett. Maximum entropy with nonlinear constraints: physical examples. In [208], pages 243–249. 1990.
115. Piero Giovanni Luca Porta Mana. On the relation between plausibility logic and the maximum-entropy principle: a numerical study, 2009. [arXiv:0911.2197](#). Also presented as invited talk at the 31st International Workshop on Bayesian Inference and Maximum Entropy Methods in Science and Engineering ‘MaxEnt 2011’, Waterloo, Canada.
116. B. Roy Frieden. Statistical models for the image restoration problem. *Comput. Graph. Image Process.*, 12:40–59, 1980.
117. Edwin Thompson Jaynes. Monkeys, kangaroos, and  $N$ . In [220], pages 26–58, 1986. See also the rev. and corrected version [35].
118. James O. Berger. *Statistical Decision Theory and Bayesian Analysis*. Springer series in statistics. Springer, New York, 2 edition, 1985. First publ. 1980.
119. José-Miguel Bernardo and Adrian F. Smith. *Bayesian Theory*. Wiley series in probability and mathematical statistics. John Wiley & Sons, Chichester, 1994.
120. Andrew Gelman, John B. Carlin, Hal S. Stern, and Donald B. Rubin. *Bayesian Data Analysis*. Texts in statistical science. Chapman & Hall/CRC, Boca Raton, USA, 2 edition, 2004. First publ. 1995.
121. Arnold Zellner. *An Introduction to Bayesian Inference in Econometrics*. Wiley classics library. John Wiley & Sons, New York, 1996. First publ. 1971.
122. Mike West and Jeff Harrison. *Bayesian Forecasting and Dynamic Models*. Springer series in statistics. Springer, New York, 2 edition, 1997. First publ. 1989.
123. John Skilling. Classic maximum entropy. In [221], pages 45–52. 1989.
124. Carlos C. Rodríguez. Entropic priors, 1991. <http://omega.albany.edu:8008/>.
125. Ariel Caticha. Maximum entropy, fluctuations and priors. *Am. Inst. Phys. Conf. Proc.*, 568:94–105, 2001. [arXiv:math-ph/0008017](#).
126. Carlos C. Rodríguez. Entropic priors for discrete probabilistic networks and for mixtures of Gaussians models, 2002. [arXiv:physics/0201016](#); <http://omega.albany.edu:8008/>.
127. Carlos C. Rodríguez. A geometric theory of ignorance, 2003. <http://omega.albany.edu:8008/>.
128. Ariel Caticha and Roland Preuss. Maximum entropy and Bayesian data analysis: Entropic prior distributions. *Phys. Rev. E*, 70(4):046127, 2004. [arXiv:physics/0307055](#).

129. John A. Hertz, Yasser Roudi, and Joanna Tyrcha. Ising models for inferring network structure from spike data. In [13], chapter 27, pages 527–546. 2013. First publ. 2011 as [arXiv:1106.1752](https://arxiv.org/abs/1106.1752).
130. Edwin Thompson Jaynes. Where do we stand on maximum entropy? In [211], pages 15–118. 1979. <http://bayes.wustl.edu/etj/node1.html>; repr. with an introduction in [204], pp. 210–314.
131. Edwin Thompson Jaynes. The minimum entropy production principle. *Annu. Rev. Phys. Chem.*, 31:579, 1980. <http://bayes.wustl.edu/etj/node1.html>.
132. Edwin Thompson Jaynes. Macroscopic prediction. In [222], pages 254–269. 1985. Updated version 1996 at <http://bayes.wustl.edu/etj/node1.html>.
133. Walter T. Grandy, Jr. *Entropy and the Time Evolution of Macroscopic Systems*, volume 141 of *International series of monographs on physics*. Oxford University Press, Oxford, 2008.
134. Julian Lee and Steve Pressé. A derivation of the master equation from path entropy maximization. *J. Chem. Phys.*, 137(7):074103, 2012.
135. Steve Pressé, Kingshuk Ghosh, Julian Lee, and Ken A. Dill. Principles of maximum entropy and maximum caliber in statistical physics. *Rev. Mod. Phys.*, 85(3):1115–1141, 2013. [http://statphysbio.physics.iupui.edu/Presse\\_rmp.pdf](http://statphysbio.physics.iupui.edu/Presse_rmp.pdf).
136. R. B. Potts. Note on the factorial moments of standard distributions. *Aust. J. Phys.*, 6(4):498–499, 1953.
137. Wilhelm Lenz. Beitrag zum Verständnis der magnetischen Erscheinungen in festen Körpern. *Physik. Zeitschr.*, XXI:613–615, 1920. [http://www.physik.uni-rostock.de/fileadmin/Physik/Mahnke/Geschichte/Wilhelm\\_Lenz/Lenz\\_1920.pdf](http://www.physik.uni-rostock.de/fileadmin/Physik/Mahnke/Geschichte/Wilhelm_Lenz/Lenz_1920.pdf).
138. Ernst Ising. Beitrag zur Theorie des Ferromagnetismus. *Z. Phys.*, 31(1):253–258, 1925.
139. Rudolf E. Peierls. Quelques propriétés typiques des corps solides. *Ann. Inst. Henri Poincaré*, 5(3):177–222, 1935.
140. Lars Onsager. Crystal statistics. I. A two-dimensional model with an order-disorder transition. *Phys. Rev.*, 65(3–4):117–149, 1944.
141. Kyozi Kawasaki. Kinetics of Ising models. In [223], chapter 11, pages 443–501. 1972.
142. David Sherrington and Scott Kirkpatrick. Solvable model of a spin-glass. *Phys. Rev. Lett.*, 35(26):1792–1796, 1975.

143. Scott Kirkpatrick and David Sherrington. Infinite-ranged models of spin-glasses. *Phys. Rev. B*, 17(11):4384–4403, 1978.
144. Josiah Willard Gibbs. *Elementary Principles in Statistical Mechanics: Developed with Especial Reference to the Rational Foundation of Thermodynamics*. Charles Scribner’s Sons, New York, 1902. <http://gallica.bnf.fr/notice?N=FRBNF37257076>; repr. in [224].
145. Gérard G. Emch and Chuang Liu. *The Logic of Thermostatistical Physics*. Springer, Berlin, 2002.
146. Roger Balian. *From Microphysics to Macrophysics: Methods and Applications of Statistical Physics. Vol. I*. Theoretical and mathematical physics. Springer, Berlin, 2nd printing edition, 2007. Transl. by D. ter Haar and J. F. Gregg; first publ. in French 1982.
147. Roger Balian. *From Microphysics to Macrophysics: Methods and Applications of Statistical Physics. Vol. II*. Theoretical and mathematical physics. Springer, Berlin, 2nd printing edition, 2007. Transl. by D. ter Haar; first publ. in French 1982.
148. Walter T. Grandy, Jr. *Foundations of Statistical Mechanics. Vol. I: Equilibrium Theory*. Fundamental theories of physics. D. Reidel, Dordrecht, 1987.
149. Walter T. Grandy, Jr. *Foundations of Statistical Mechanics. Vol. II: Nonequilibrium Phenomena*. Fundamental theories of physics. D. Reidel, Dordrecht, 1988.
150. Arthur Hobson. Irreversibility in simple systems. *Am. J. Phys.*, 34:411–416, 1966.
151. Arthur Hobson and David N. Loomis. Exact classical nonequilibrium statistical-mechanical analysis of the finite ideal gas. *Phys. Rev.*, 173(1):285–295, 1968. [http://ergodic.ugr.es/statphys\\_grado/bibliografia/hoobson.pdf](http://ergodic.ugr.es/statphys_grado/bibliografia/hoobson.pdf).
152. Arthur Hobson. *Concepts in Statistical Mechanics*. Gordon and Breach, New York, 1971.
153. Christian Maes and Karel Netočný. Time-reversal and entropy. *J. Stat. Phys.*, 110(1–2):269–310, 2003. [arXiv:cond-mat/0202501](https://arxiv.org/abs/cond-mat/0202501).
154. James Clerk Maxwell. Introductory lecture on experimental physics, 1871. Repr. in [225], pp. 241–255.
155. James Clerk Maxwell. On the dynamical evidence of the molecular constitution of bodies. *Nature*, XI(279, 280):357–359, 374–377, 1875. Repr. in [225], pp. 418–438.
156. James Clerk Maxwell. Tait’s “Thermodynamics”. *Nature*, 17(431, 432):257–259, 278–280, 1878. Repr. in [225], pp. 660–671.

157. Albert Einstein. Kinetische Theorie des Wärmegleichgewichtes und des zweiten Hauptsatzes der Thermodynamik. *Ann. der Phys.*, 9:417–433, 1902. Repr. in [226], transl. in [227].
158. David J. C. MacKay. Bayesian interpolation. *Neural Comp.*, 4(3):415–447, 1992. <http://www.inference.phy.cam.ac.uk/mackay/PhD.html>.
159. Harold Grad. Statistical mechanics of dynamical systems with integrals other than energy. *J. Phys. Chem.*, 56(9):1039–1048, 1952. See also [228].
160. Harold Grad. The many faces of entropy. *Comm. Pure Appl. Math.*, 14:323–354, 1961.
161. Harold Grad. Levels of description in statistical mechanics and thermodynamics. In [205], chapter 5, pages 49–76. 1967.
162. Edwin Thompson Jaynes. The Gibbs paradox. In C. R. Smith, G. J. Erickson, and P. O. Neudorfer, editors, *Maximum-Entropy and Bayesian Methods*, pages 1–22. Kluwer Academic, Dordrecht, 1992. <http://bayes.wustl.edu/etj/node1.html>.
163. Joel L. Lebowitz and Christian Maes. Entropy: a dialogue. In [209], chapter 13, pages 269–276. 2003.
164. Alexa Riehle, Sarah Wirtsohn, Sonja Grün, and Thomas Brochier. Mapping the spatio-temporal structure of motor cortical lfp and spiking activities during reach-to-grasp movements. *Front. Neural Circuits*, 7:48, 2013. doi: 10.3389/fncir.2013.00048.
165. Kevin H. Knuth. Optimal data-based binning for histograms, 2013. [arXiv:physics/0605197](https://arxiv.org/abs/physics/0605197). First publ. 2006.
166. Carl van Vreeswijk and Haim Sompolinsky. Chaos in neuronal networks with balanced excitatory and inhibitory activity. *Science*, 274:1724–1726, December, 6 1996.
167. J. J. Binney, N. J. Dowrick, A. J. Fischer, and M. E. J. Newman. *The Theory of Critical Phenomena: An Introduction to the Renormalization Group*. Oxford University Press, Oxford, 2001. First publ. 1992.
168. Manfred Oppen and Ole Winther. From naive mean field theory to the TAP equations. In [75], chapter 2, pages 7–20. 2001. <http://cogsys.imm.dtu.dk/staff/winther/oppen.fromnaive.pdf>.
169. Shun-ichi Amari, Shiro Ikeda, and Hidetoshi Shimokawa. Information geometry of  $\alpha$ -projection in mean field approximation. In [75], chapter 16. 2001. <http://www.ism.ac.jp/~shiro/papers/techreport/TR2000-6.pdf>.
170. Toshiyuki Tanaka. Information geometry of mean-field approximation. In [75], chapter 17, pages 259–273. 2001.

171. Milton Abramowitz and Irene A. Stegun, editors. *Handbook of Mathematical Functions: With Formulas, Graphs, and Mathematical Tables*, volume 55 of *National Bureau of Standards Applied mathematics series*. U.S. Department of Commerce, Washington, D.C., tenth printing, with corrections edition, 1972. First publ. 1964.
172. Keit B. Oldham, Jan C. Myland, and Jerome Spanier. *An Atlas of Functions: with Equator, the Atlas Function Calculator*. Springer, New York, 2 edition, 2009. First publ. 1987.
173. K. H. Fischer and J. A. Hertz. *Spin glasses*, volume 1 of *Cambridge studies in magnetism*. Cambridge University Press, Cambridge, reprint edition, 1993. First publ. 1991.
174. Wyeth Bair, Ehud Zohary, and William T. Newsome. Correlated firing in macaque visual area MT: Time scales and relationship to behavior. *J. Neurosci.*, 21(5):1676–1697, 2001. [http://invibe.net/biblio\\_database\\_dyva/woda/data/att/fc5e.file.pdf](http://invibe.net/biblio_database_dyva/woda/data/att/fc5e.file.pdf).
175. Mark E. Mazurek and Michael N. Shadlen. Limits to the temporal fidelity of cortical spike rate signals. *Nat. Neurosci.*, 5(5):463–471, 2002. [https://www.shadlenlab.columbia.edu/publications/publications/mike/mazurek\\_shadlen2002.pdf](https://www.shadlenlab.columbia.edu/publications/publications/mike/mazurek_shadlen2002.pdf).
176. Adam Kohn and Matthew A. Smith. Stimulus dependence of neuronal correlation in primary visual cortex of the macaque. *J. Neurosci.*, 25(14):3661–3673, 2005. <http://www.smithlab.net/publications.html>.
177. Matthew A. Smith and Adam Kohn. Spatial and temporal scales of neuronal correlation in primary visual cortex. *J. Neurosci.*, 28(48):12591–12603, 2008. <http://www.smithlab.net/publications.html>.
178. Konstantin I. Bakhurin, Victor Mac, Peyman Golshani, and Sotiris C. Masmanidis. Temporal correlations among functionally specialized striatal neural ensembles in reward-conditioned mice. *J. Neurophysiol.*, 115(3):1521–1532, 2016.
179. David Fowler. The binomial coefficient function. *Am. Math. Monthly*, 103(1):1–17, 1996.
180. Gašper Tkačik, Olivier Marre, Thierry Mora, Dario Amodei, Michael J. Berry II, and William Bialek. The simplest maximum entropy model for collective behavior in a neural network. *J. Stat. Mech.*, 2013:P03011, 2013. [arXiv:1207.6319](https://arxiv.org/abs/1207.6319).
181. Gašper Tkačik, Olivier Marre, Dario Amodei, Elad Schneidman, William Bialek, and Michael J. Berry II. Searching for collective behavior in a large network of sensory neurons. *PLoS Computational Biology*, 10(1):e1003408, 2014. [arXiv:1306.3061](https://arxiv.org/abs/1306.3061).

182. William Feller. *An Introduction to Probability Theory and Its Applications. Vol. I.* Wiley series in probability and mathematical statistics. John Wiley & Sons, New York, 3 edition, 1968. First publ. 1950.
183. Sheldon Ross. *A First Course in Probability.* Pearson, Upper Saddle River, USA, 8 edition, 2010. First publ. 1976.
184. David H. Wolpert and David R. Wolf. Estimating functions of probability distributions from a finite set of samples, part 1: Bayes estimators and the Shannon entropy, 1994. [arXiv:comp-gas/9403001](#), see also [185, 186].
185. David H. Wolpert and David R. Wolf. Estimating functions of distributions from a finite set of samples, part 2: Bayes estimators for mutual information, chi-squared, covariance and other statistics, 1994. [arXiv:comp-gas/9403002](#), see also [184, 186].
186. David H. Wolpert and David R. Wolf. Estimating functions of probability distributions from a finite set of samples. *Phys. Rev. E*, 52(6):6841–6854, 1995. See also erratum [229] and [184, 185].
187. Malay Ghosh and Glen Meeden. *Bayesian Methods for Finite Population Sampling*, volume 79 of *Monographs on statistics and applied probability*. Springer, Dordrecht, reprint edition, 1997.
188. Piero Giovanni Luca Porta Mana, Emiliano Torre, and Vahid Rostami. Inferences from a network to a subnetwork and vice versa under an assumption of symmetry, 2015. [bioRxiv:2015/12/11/034199](#).
189. Kurt Binder. Applications of Monte Carlo methods to statistical physics. *Rep. Prog. Phys.*, 60(5):487–559, 1997. [http://fisica.ciencias.uchile.cl/~gonzalo/cursos/SimulacionII/rpphys\\_binder97.pdf](http://fisica.ciencias.uchile.cl/~gonzalo/cursos/SimulacionII/rpphys_binder97.pdf).
190. Edwin Thompson Jaynes. Bayesian methods: general background. In [220], pages 1–25, 1986. <http://bayes.wustl.edu/etj/node1.html>.
191. Thomas Bayes. An essay towards solving a problem in the doctrine of chances. *Phil. Trans. R. Soc. Lond.*, 53:370–418, 1763. <http://www.stat.ucla.edu/history/essay.pdf>; with an introduction by Richard Price. The *Scholium* of p. 392 is reprinted and analysed in [230].
192. Pierre Simon Laplace, (Marquis de). *Essai philosophique sur les probabilités.* Courcier, Paris, 4 edition, 1819. Repr. as the Introduction of [231], pp. V–CLIII; <http://gallica.bnf.fr/document?0=N077595>.
193. John Skilling. Theory of maximum entropy image reconstruction. In [220], pages 156–178. 1986.
194. Nicholas Weir. Applications of maximum entropy techniques to HST data. In [232], pages 115–129. 1991.

195. John Skilling and R. K. Bryan. Maximum entropy image reconstruction: general algorithm. *Mon. Not. Roy. Astron. Soc.*, 211(1):111–124, 1984.
196. F. P. Kelly. *Reversibility and Stochastic Networks*. John Wiley & Sons, Chichester, 1979. [http://www.statslab.cam.ac.uk/~frank/B00KS/kelly\\_book.html](http://www.statslab.cam.ac.uk/~frank/B00KS/kelly_book.html).
197. N. G. van Kampen. *Stochastic Processes in Physics and Chemistry*. North-Holland, Amsterdam, 3 edition, 2007. First publ. 1981.
198. Crispin W. Gardiner. *Handbook of Stochastic Methods: for Physics, Chemistry and the Natural Sciences*. Springer series in synergetics. Springer, Berlin, 3 edition, 2004. First publ. 1983.
199. Giorgio Koch and Fabio Spizzichino, editors. *Exchangeability in Probability and Statistics: Proceedings of the International Conference on Exchangeability in Probability and Statistics*. North-Holland, Amsterdam, 1982.
200. Paul Damien, Petros Dellaportas, Nicholas G. Polson, and David A. Stephens, editors. *Bayesian Theory and Applications*. Oxford University Press, Oxford, 2013.
201. Claude Elwood Shannon. Communication in the presence of noise. *Proc. IEEE*, 86(2):447–457, 1998. Repr. of [22], with an introduction [23].
202. Edwin Thompson Jaynes. Information theory and statistical mechanics. II. *Phys. Rev.*, 108(2):171–190, 1957. <http://bayes.wustl.edu/etj/node1.html>, see also [23].
203. K. W. Ford, editor. *Statistical Physics*, volume 3 of *1962 Brandeis Summer Institute lectures in theoretical physics*. W. A. Benjamin, New York, 1963.
204. Edwin Thompson Jaynes. *E. T. Jaynes: Papers on Probability, Statistics and Statistical Physics*. Kluwer Academic, Dordrecht, reprint edition, 1989. Ed. by R. D. Rosenkrantz. First publ. 1983.
205. Mario Bunge, editor. *Delaware Seminar in the Foundations of Physics*, volume 1 of *Studies in the foundations: methodology and philosophy of science*. Springer, Berlin, 1967.
206. C. Ray Smith and Walter T. Grandy, Jr., editors. *Maximum-Entropy and Bayesian Methods in Inverse Problems*. Fundamental theories of physics. D. Reidel, Dordrecht, 1985.
207. José-Miguel Bernardo, M. H. DeGroot, D. V. Lindley, and A. F. M. Smith, editors. *Bayesian Statistics 2: Proceedings of the Second Valencia International Meeting*. Elsevier and Valencia University Press, Amsterdam and Valencia, 1985.

208. Paul F. Fougère, editor. *Maximum Entropy and Bayesian Methods: Dartmouth, U.S.A., 1989*, volume 39 of *Fundamental theories of physics*. Kluwer Academic, Dordrecht, 1990.
209. Andreas Greven, Gerhard Keller, and Gerald Warnecke, editors. *Entropy*. Princeton series in applied mathematics. Princeton University Press, Princeton and Oxford, 2003.
210. Jonathon Shlens, Greg D. Field, Jeffrey L. Gauthier, Matthew I. Grivich, Dumitru Petrusca, Alexander Sher, Alan M. Litke, and E. J. Chichilnisky. Correction, the structure of multi-neuron firing patterns in primate retina. *J. Neurosci.*, 28(5): 1246, 2008. See [47].
211. Raphael D. Levine and Myron Tribus, editors. *The Maximum Entropy Formalism: A Conference Held at the Massachusetts Institute of Technology on May 2–4, 1978*. The MIT Press, Cambridge, USA, 1979.
212. David E. Rumelhart, James L. McClelland, and the PDP Research Group. *Parallel Distributed Processing: Explorations in the Microstructure of Cognition. Vol. 1: Foundations*. Computational models of cognition and perception. The MIT Press, Cambridge, USA, 12th printing edition, 1999. First publ. 1986.
213. Douglas Rayne Hartree. The wave mechanics of an atom with a non-coulomb central field. Part II. Some results and discussion. *Proc. Cambridge Philos. Soc.*, 24(1):111–132, 1928. <http://sci-prew.inf.ua/index1.htm>; see [73].
214. P. R. Krishnaiah and P. K. Sen, editors. *Handbook of Statistics 4: Nonparametric Methods*. North-Holland, Amsterdam, 1984.
215. Jerzy Neyman, editor. *Proceedings of the Fourth Berkeley Symposium on Mathematical Statistics and Probability, Held at the Statistical Laboratory, University of California, June 20–July 30, 1960. Vol. I: Contributions to the Theory of Statistics*. University of California Press, Berkeley and Los Angeles, 1961.
216. J. A. Roberts, editor. *Indirect Imaging: Measurement and processing for indirect imaging (Proceedings of an International Symposium, Sydney, Australia, 30 August to 2 September 1983)*. Cambridge University Press, Cambridge, 1984.
217. Joint Committee for Guides in Metrology (JCGM). *JCGM 102:2011: Evaluation of measurement data – Supplement 2 to the “Guide to the expression of uncertainty in measurement” – Extension to any number of output quantities*. BIPM, IEC, IFCC, ILAC, ISO, IUPAC, IUPAP, OIML, 2011. <http://www.bipm.org/en/publications/guides/gum.html>. See [105].
218. Joint Committee for Guides in Metrology (JCGM). *JCGM 104:2009: Evaluation of measurement data – An introduction to the “Guide to the expression of uncertainty*

- in measurement" and related documents.* BIPM, IEC, IFCC, ILAC, ISO, IUPAC, IUPAP, OIML, 2012. <http://www.bipm.org/en/publications/guides/gum.html>. See [105].
219. Joint Committee for Guides in Metrology (JCGM). *JCGM 106:2012: Evaluation of measurement data – The role of measurement uncertainty in conformity assessment.* BIPM, IEC, IFCC, ILAC, ISO, IUPAC, IUPAP, OIML, 2012. <http://www.bipm.org/en/publications/guides/gum.html>. See [105].
  220. James H. Justice, editor. *Maximum Entropy and Bayesian Methods in Applied Statistics: Proceedings of the Fourth Maximum Entropy Workshop, University of Calgary, 1984.* Cambridge University Press, Cambridge, 2008. First publ. 1986.
  221. John Skilling, editor. *Maximum Entropy and Bayesian Methods: Cambridge, England, 1988.* Fundamental theories of physics. Kluwer Academic, Dordrecht, 1989.
  222. Hermann Haken, editor. *Complex Systems – Operational Approaches: in Neurobiology, Physics, and Computers. Proceedings of the International Symposium on Synergetics at Schloß Elmau, Bavaria, May 6–11, 1985,* volume 31 of *Springer series in synergetics.* Springer, Berlin, 1985.
  223. C. Domb and M. S. Green, editors. *Phase Transitions and Critical Phenomena. Vol. 2.* Academic Press, London, 1972.
  224. Josiah Willard Gibbs. *The Collected Works of J. Willard Gibbs. Vol. II: Statistical Mechanics and Dynamics.* Longmans, Green and Co., New York, 1928. First publ. 1906.
  225. James Clerk Maxwell. *The Scientific Papers of James Clerk Maxwell. Vol. Two.* Dover, New York, 1965. Ed. by W. D. Niven. Two volumes bound as one. <http://num-scd-ulp.u-strasbg.fr:8080/347/>. First publ. 1890.
  226. Albert Einstein. Kinetische Theorie des Wärmegleichgewichtes und des zweiten Hauptsatzes der Thermodynamik. *Ann. der Phys.*, 14(S1):117–134, 2005.
  227. Albert Einstein. Kinetic theory of thermal equilibrium and of the second law of thermodynamics. In [234], pages 30–47. 1989.
  228. Harold Grad. Statistical mechanics, thermodynamics, and fluid dynamics of systems with an arbitrary number of integrals. *Comm. Pure Appl. Math.*, 5(4):455–494, 1952. See also [159].
  229. David H. Wolpert and David R. Wolf. Erratum: Estimating functions of probability distributions from a finite set of samples. *Phys. Rev. E*, 54(6):6973, 1996. See [186].

230. Stephen M. Stigler. Thomas Bayes's Bayesian inference. *J. Roy. Stat. Soc. A*, 145 (2):250–258, 1982.
231. Pierre Simon Laplace, (Marquis de). *Théorie analytique des probabilités*. Courcier, Paris, 3 edition, 1820. First publ. 1812; repr. in [235]; <http://gallica.bnf.fr/document?O=N077595>.
232. P. J. Grosbøl and R. H. Warmels, editors. *Third ESO/ST-EFC Data Analysis Workshop, held in Garching, 22–23 April, 1991*. Number 38 in ESO conference and workshop proceedings. European Southern Observatory, Garching, 1991.
233. Aaron D. Wyner and Shlomo Shamai. Introduction to “Communication in the presence of noise”. *Proc. IEEE*, 86(2):442–446, 1998. See [201].
234. Albert Einstein. *The Collected Papers of Albert Einstein. Vol. 2: The Swiss Years: Writings, 1900–1909. (English translation)*. Princeton University Press, Princeton, 1989. Transl. by Anna Beck and Peter Havas; <http://einsteinpapers.press.princeton.edu/>.
235. Pierre Simon Laplace, (Marquis de). *Œuvres complètes de Laplace. Tome septième: Théorie analytique des probabilités*. Gauthier-Villars, Paris, 1886. ‘Publiées sous les auspices de l’Académie des sciences, par MM. les secrétaires perpétuels’; <http://gallica.bnf.fr/notice?N=FRBNF30739022>.